A Review and Perspective on Optical Phased Array for Automotive LiDAR

Ching-Pai Hsu, Boda Li, Braulio Solano-Rivas, Amar R Gohil, Pak Hung Chan, Andrew D Moore and Valentina Donzella

***Abstract*—This paper aims to review the state of the art of Light Detection and Ranging (LiDAR) sensors for automotive applications, and particularly for automated vehicles, focusing on recent advances in the field of integrated LiDAR, and one of its key components: the Optical Phased Array (OPA). LiDAR is still a sensor that divides the automotive community, with several automotive companies investing in it, and some companies stating that LiDAR is a 'useless appendix'. However, currently there is not a single sensor technology able to robustly and completely support automated navigation. Therefore, LiDAR, with its capability to map in 3 dimensions (3D) the vehicle surroundings, is a strong candidate to support Automated Vehicles (AVs). This manuscript highlights current AV sensor challenges, and it analyses the strengths and weaknesses of the perception sensor currently deployed. Then, the manuscript discusses the main LiDAR technologies emerging in automotive, and focuses on integrated LiDAR, challenges associated with light beam steering on a chip, the use of Optical Phased Arrays, finally discussing current factors hindering the affirmation of silicon photonics OPAs and their future research directions.**

***Index Terms*—Optical Phased Array, Intelligent Vehicles, Silicon Photonics, LiDAR, Autonomous and Automated Vehicles.**

I. Introduction

The Society of Automotive Engineers, SAE, have described in their standard SAE-J3016 six levels of vehicle autonomy, from level 0 to level 5 (L0-L5) [1]. In L0 (No Automation), the vehicle function/system does not interfere with the driving tasks (completely managed by the driver), but can deliver helpful information to the driver via sounds, displays, haptic, i.e. in Blind Spot Monitoring. On the opposite side, in L5 (Full Automation), the vehicle system can accomplish all the driving tasks, everywhere and at all times, relying on the sensors to perceive the environment, and even able to implement a minimal risk maneuver (MRM) in case of sensor/system failure. Between these two extremes, there are intermediate levels of autonomy; each one of them is rigorously defined in the SAE standard [1].

As the level of autonomy increases, the situation awareness of the vehicle needs to improve, and extensive and robust sensor coverage is required, particularly for Automated Vehicles (AVs, L3 and above). Currently, all the environmental perception sensor technologies have strengths and weaknesses (par. II.F), and a single sensor technology is not able to safely and robustly support perception for AVs. Amongst the perception sensors, LiDAR still divides the automotive community and its stakeholders, and there are several different LiDAR technologies competing for market supremacy. Fully integrated Optical Phased Array LiDAR, based on miniaturized antennas on Silicon chips will be the focus of this paper.

Manuscript received April 14, 2020.

Ching-Pai Hsu, Boda Li, Braulio Solano-Rivas, Amar Gohil, Pak Hung Chan, Andrew D Moore and Valentina Donzella are with WMG, University of Warwick, CV4 9JB, Coventry UK (corresponding author e-mail: v.donzella@warwick.ac.uk).

A. Situation awareness and sensor coverage

Situation awareness for vehicles is *understanding* the environment in a certain volume of space and time around the vehicle [2]. The needed spatial and temporal sensor coverage grows as the level of Autonomy increases. In particular, at L4 and L5, the vehicle surroundings need to be completely covered, with data rates adequate to the vehicle speed; there is also the need of having sensor coverage redundancy, to mitigate risks in case of fallback, and to guarantee coverage with adverse weather, low light conditions, malfunctions, etc., [3]-[4]. An accurate 3D reconstruction of the environment and the objects around the vehicle (including their range and relative speed, size and position/direction) is key for building a suitable understanding of the environment.

We can define the *sensor spatial coverage* as the combination of its horizontal and vertical field of view (HFoV and VFoV) and its detection range (R_{max}). Ideally, an object situated in the volume between the maximum detection range and in its HFoV and VFoV will be detected (red region in Fig.1a). However, the accuracy, resolution and sensitivity of the measurement will change in this volume, generally degrading when the target distance from the ego-vehicle (therefore from the sensor) is increasing. LiDAR can strongly support the vehicle sensor suite to gather 3D spatial information in the form of a pointcloud, Fig.1b [5]-[6]. The *sensor temporal coverage* depends on the data-rate, and on how many new sensor measurements per second are available to the vehicle system.

B. Resolution, Detection, Identification and Tracking

The sensor resolution is the smallest variation in the entity under measurement that will cause a change in the sensor output. It defines the limit of which variations can be detected by a specific environmental perception sensor.

Furthermore, with environmental perception sensors, it is worth clarifying what we mean with target detection, target

identification and target tracking; usually their combination makes the sensor output more reliable. The target detection is the existence of a generic object in front of the sensor, different from the background and other elements. The target identification is to recognize that the detected object belongs to a specific category, e.g. vulnerable road users, vehicles, trucks. Tracking is the ability to associate an object in the previous reading with the current reading, and therefore assigning a path to that specific object. Classification and tracking are important assets of environmental perception sensors, because they can be used to predict future plausible movements of road users, and therefore evaluate a safe path for the ego-vehicle.

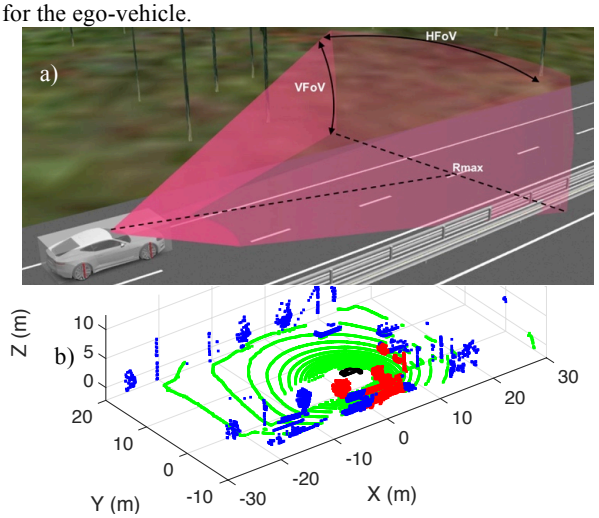

Fig. 1. (a) Simplified representation of the spatial coverage by a generic environmental perception sensor, highlighted by the red volume in the figure. (b) Example of 3D LiDAR pointcloud, segmented, modified from [5].

C. AVs and sensing challenges

Currently there are several challenges associated with the sensor suite of AVs, in this section we discuss some of them.

- Sensor performance dependence on environmental/weather conditions [7-8]. Sensor performance degradation needs to be consistent and predictable under changing environmental conditions. Moreover, the performance of different sensor technologies will vary (with different extents) according to the environmental conditions (see par. II.F and par. III.A). Furthermore, temperature management is fundamental in automotive, as electronic devices are required to work between −40 °C to 125 °C; these temperature variations can be extremely critical for solid state LiDAR (see par. V.E).
- Identification of small targets (e.g. potholes, animals, person lying down on the ground) and vulnerable road users (cyclist, pedestrian) [9]. Sensors not only need to have high enough resolution to detect these entities, but also to be able to identify/classify them and to track them.
- Uncertainty on the measurement. Each sensor has an estimated error on the datasheet [10]-[11]; however, there are few techniques to estimate how these uncertainties change due to intrinsic and extrinsic noise, and therefore to estimate the overall uncertainty on the measured value.
- False positives and false negatives [12]. False positive is a wrong sensor output that indicates the presence of a target while it actually does not exist. False negative is a failure in detecting a real target in time when the target does exist and must be sensed. False positives and false negatives can affect different sensor technologies for reasons like dynamic environment, spurious or multiple detection, hardware failures or software errors, and deliberate hacking [13].
- Sensor fusion. Different sensor technologies will provide data in different formats at different rates, with different resolution and uncertainties. There are several ways of combing the data, but they are computational expensive and require a deep understanding of sensor working principles.
- Corner or edge cases. To demonstrate that AVs are safer than human driver, with enough confidence in the measurement, millions of miles are requested to be driven [14]. However, it is not realistic to cover all the real-world driving scenarios, and there are always going to be some unpredictable, unforeseen or not reproducible cases (e.g. a person dressed up as a hot dog at a city fair; extremely strong rain showers). It is tremendously difficult to predict the behavior of sensors in these extreme conditions [15].
- Data amount and speed. Overall the estimated bandwidth needed for a L3 sensor suite is an outstanding 3Gbit/s-40Gbit/s [16], and current automotive networks cannot cope with the required bandwidth [17-18].
- Redundancy versus complexity. Redundancy contributes to the robustness of the system. However, redundancy increases: (1) the amount of data (not desirable, as stated in previous point); (2) weight and cost (as more components are needed); (3) complexity of the sensor fusion algorithms; (4) required computational power; (5) power consumption.

To conclude, AV sensor technology needs further development to meet automotive cost and safety requirements.

D. Paper structure

After covering an introduction to AVs in this section, the paper is organized as follows: section II reviews the state of the art of AV environmental perception sensors, focusing on their strengths and weaknesses; section III discusses LiDAR technologies in details; section IV analyzes current research on optical phased array (OPA) LiDAR; section V evaluates the OPA-LiDAR technical challenges and research trends.

TABLE I
OVERVIEW OF THE ENVIRONMENTAL PERCEPTION SENSORS. US (FIRST ROW IN LIGHT BLUE) ARE BASED ON SOUND WAVES; THE OTHER SENSORS (VIOLET ROWS) USE ELECTROMAGNETIC (EM) WAVES AT DIFFERENT FREQUENCIES.

Technology	Waveband	Typical Applications
Ultrasonic	>40kHz (SOUND WAVES)	Parking sensors, detection in short range (<10m) [19-20].
RADAR	24GHz (temporary) 77 GHz to 81 GHz	Collision detection/avoidance Distance and speed meas. [21]
LiDAR	1550nm – 530nm	3D Depth Mapping, distance measurements [22-23]
Camera (Infrared)	15000nm – 1000nm 1400nm – 700nm	Night vision, person/animal identification [24-25]
Camera (visible)	700nm – 380nm	Object detection, trajectory prediction, sign recognition. [25]

II. AUTOMOTIVE ENVIRONMENTAL PERCEPTION SENSORS

Modern vehicles are equipped with numerous sensors, used for manifold reasons, for example: to monitor vehicle dynamics and status (e.g. accelerometers, wheel speed sensors, etc.); for comfort (e.g. in cabin temperature sensor); for localization (e.g. GPS, GNSS); and, as discussed, the sensors deployed to understand the vehicle surroundings. This last category is named as '*environmental perception sensors*', and it includes all sensors that perceive targets through measuring physical signals, mainly in the form of ultra-sound (US) waves or electromagnetic (EM) waves. A review of these sensors, listed in Table I, is given in the following paragraphs.

A. Visible camera

Complementary Metal Oxide Semiconductor (CMOS) cameras are commonly used perception sensors [26], as they offer relatively low cost, ease of installation and ability to perceive colors, textures and contrasts [27]-[28]. Visible light is focused through specific lenses, decomposed into colors, and acquired as an electric signal. A traditional way of decomposing visible light is to use the Bayer filter, a red-green-green-blue (RGGB) 2x2 pixel matrix. However, in automotive, other solutions have been explored, Fig.2 [29]. The resolution of the final image can be determined by two variables: spatial and tonal. The spatial resolution is directly related to the pixel density of the image sensor that is measured in Pixels-per-inch (PPI); the tonal resolution is measured by the configured color representation values set in the sensor and its dynamic range [30].

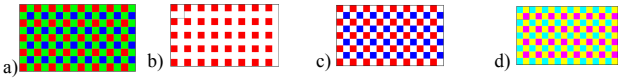

Fig. 2. Schematic representation of CMOS camera pixel arrays with different filter options (each small colored square represents the color filter of one pixel, if the square is white, no color filter is applied to that pixel): (a) Bayer filter (RGGB); (b) RCCC; (c) RCCB; (d) CYYM.

Within the types of cameras used in automotive, there are monocular, stereo, and depth cameras (RGB-D) [31], [32].

B. Infrared (IR) sensors

Infrared or thermal sensors/cameras have a detector working similarly to regular cameras (a pixel array), but in this case pixels are sensitive to EM waves in the near or far infrared (NIR and FIR). These sensors allow to detecting objects (particularly living beings or warm/hot objects), under low light conditions and through mist and smoke [33]. Detection is relatively unaffected at night and dawn or dusk that can cause respectively high amounts of noisy artifacts or blooming effects in traditional cameras [34]. However, the shift in working frequency increases the cost and size of the sensors.

IR sensors can be broadly divided into two categories:

- Passive type – they have pixels based on microbolometers and detect FIR object energy emitted in the form of black body radiation [35]-[36]. This mechanism makes it extremely easy to detect most living beings, and maximum range, R_{max}, can be more than 300 m.
- Active type - they emit light in the NIR and detected the light reflected back by the objects [37]. Detector technology is cheaper with respect to microbolometers, but range is limited by the need to transmit and receive a reflected back NIR wave (R_{max} is around 100 m).

C. Ultrasonic sensors (US)

US sensors are used to detect objects in close vehicle proximity, most commonly as inputs for parking assist and side view features [38]. They allow detection of objects/targets as close as 10-15 cm, in contrast to other perception sensors (and particularly of LiDAR and RADAR, usually unable to detect objects closer than 0.5m-1m). However, the coverage of the sensor is limited, with typical HFoV and VFoV of 120°-140° and 60°-80° respectively, and R_{max} around 5-6 m [39]. They are cost effective, have small size, and are easily integrated into vehicle bumpers. The basic working principle to measure the object distance is time of flight (ToF), Eq. 1, where v_{sound} is the sound wave speed in air (i.e. 343 m/s at 20°C, 101kPa), t is the time of flight for a transmitted pulse to return to the US sensor after hitting a target, and r is the distance of the object/target.

$$r=(v_{sound}\cdot t)/2 \qquad (1)$$

The performance is robust to weather [40], and US is able to detect most of the materials, but performance can degrade with sound absorbing materials, e.g. wool, fleece [41].

D. RAdio Detection And Ranging (RADAR)

RADAR is a sensor used to detect position (i.e. range) and speed of objects using radio frequency (RF) waves. In the automotive environment, RADAR is used in the 24GHz and 77GHz bands [42]. The target distance can be measured via:

- the ToF, Eq. 2 (very similar to Eq.1); c is the speed of light (i.e. $\sim 3\cdot 10^8$ m/s in vacuum), t is the time of flight for a transmitted pulse to return to the RADAR sensor after hitting a target, and r is the distance of the object.

$$r=(c\cdot t)/2 \qquad (2).$$

- deploying a signal modulated in frequency (Frequency Modulated Continuous Wave, FMCW), and using the difference in frequency between the transmitted and received back signal to calculate r (see next paragraph).

The target speed is measured using the Doppler shift, more details can be found in [43]-[44].

RADARs are based on emitting a narrow and directional radio wave beam, usually deploying some techniques to rotate this beam in the HFoV. For this reason, RADAR is reasonably accurate to measure target range and speed components in the radial direction, while accuracy is lower on the lateral direction (with uncertainties that can be in excess of 1 m).

RADAR is robust to luminosity and to adverse weather: the performance is hardly affected by medium-light rain, fog, and even snow [45]. Cost is around one thousand dollars, and covered region can vary from short range (50-100m and 120° HFoV) up to long range (>250m and ~10° HFoV), but usually VFoV is very limited, and RADAR is not suitable to measure elevation [46]. RADAR detection depends on the RADAR Cross Section (RCS) of the targets, and vulnerable road users, like pedestrians and cyclists, have small RCS and are more

difficult to be detected by RADAR [47].

E. Light Detection And Ranging

Figure 3 shows the different LiDAR technologies proposed to be used for automotive 3D LASER scanning. Except for flash LiDAR (see par. III.C), LiDARs cover the FoV (horizontally and sometimes vertically) by rotating one or more light emitter(s). This rotation of the beam can be implemented mechanically, optically, or electro-optically, as described in section III. Velodyne has been one of the first players in 3D automotive LiDAR [48]. They developed the first automotive 360° mechanically rotating LiDAR for the second DARPA (Defense Advanced Research Projects Agency) grand challenge [49]. Similarly to US and RADAR, target range can be measured by pulsed signals and ToF, Eq. 2. However, ToF is one way of performing LiDAR measurement; the other option is to use the FMCW technique, based on heterodyne detection (as mentioned for RADAR). In FMCW LiDAR, the laser beam is emitted while continuously changing its frequency with a slope S (Hz/s). The difference between the received and transmitted frequency of the signal, f_r and f_t, enables to calculate the speed, v, and the range, r, of the target, as shown Eqs.3-4, modified from [50] (λ is the transmitted signal wavelength).

$$r = \frac{c}{4S}(f_r - f_t) \quad (3)$$

$$v = \frac{\lambda}{4}(f_r + f_t) \quad (4)$$

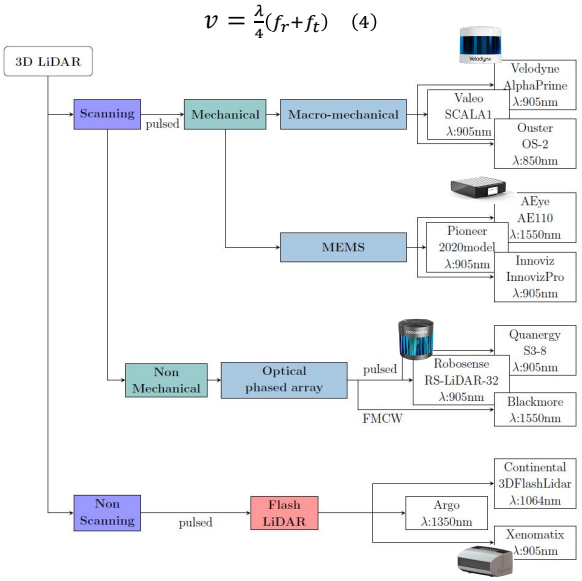

Fig. 3. Topology of different technologies used for automotive LiDAR; in the rightmost boxes there are some commercial examples [50]-[56].

Some advantages and disadvantages of ToF and FMCW LiDAR are discussed in [57]; amongst the pros of FMCW-LiDAR there is the accuracy of target speed and position measurement, as well as the decreased power requirements and the inherent capacity to reject ambient light and some environmental noises [58]. However, this technology is still under development and not ready for commercialisation [57]. In automotive LiDAR, the emitted EM beam is usually in the near infrared, the two most common wavelengths are around 905 nm and 1550 nm, and will be discussed in par. III.A.

F. Comparison of perception sensors

There are some pivotal driving factors in the selection of the environmental perception sensor suite (how many sensors, their types, and their location/coverage): cost (particularly important for passenger vehicles) and safety/robustness. The most cost-effective sensors are ultrasonic, due to their wide use in production vehicles and their mature technology. RADAR and camera costs have also been decreasing through mainstream implementation. Camera, RADAR, and US fusion has been demonstrated by companies such as Tesla as a viable solution to bring L2 functions on the road. However, Tesla autopilot has failed before due to sensor errors (e.g. as discussed in [59]), therefore the combination of US, RADAR and visible camera is not yet robust enough. LiDAR and IR sensors can complement and crosscheck the information given by other sensors, but, so far, their adoption has been hindered by elevated costs and bulkiness. However, there is the expectation that LiDAR cost and footprint will be lowered with solid-state devices (section IV-V).

In addition to the considerations above, for sensors that are based on waves emission and detection of the reflected wave, there are some materials that are transparent to specific wavelengths (e.g. the glass windows of cars or buildings can be transparent to LiDAR or RADAR beam) or can absorb the waves (e.g. fleece, woolly materials or polystyrene can absorb sound waves), and therefore can hinder the detection of some targets with specific properties. Finally, the angle between the target and the incident wave-front can deflect away the beam; surfaces that are perpendicular to the wave-front are easier to detect, particularly in the case of RADAR when few points per object are collected. LiDAR collects several points per object vertically and laterally, so it can compensate this issue.

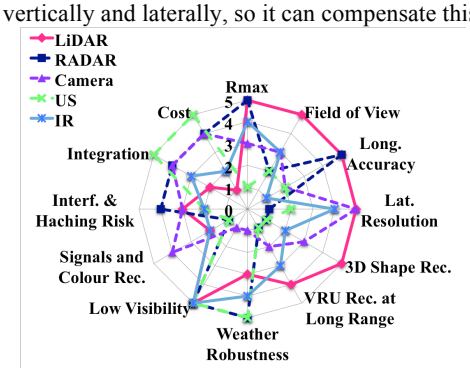

Fig. 4. Comparison of the performance of the discussed environmental perception sensors. Abbreviations: Interf., Interference; VRU, vulnerable road users; Rec., recognition; Long., longitudinal; Lat., lateral.

In Fig. 4, we have summarised some key performance indicators to compare the discussed sensors. It is clear that LiDAR is required to support robust perception, as LiDAR compensates some of the other sensor weaknesses. Moreover, it is explicit that currently sensor fusion is a key enabler for AVs, to overcome the limitations that each perception sensor has, to introduce crosschecks and plausibility checks.

III. LiDAR TECHNOLOGIES

There are several different LiDAR technologies proposed for automotive (Fig. 3). In the next chapter, we will focus on

OPA-LiDAR, while in this one we will review other technologies, starting with a discussion of used wavelengths.

A. Wavelengths

An issue that must be addressed if LiDAR is to be accepted as a key sensing technology for AVs, is the debate between which wavelength of LiDAR, λ, is best suited to the automotive environment, either around 905nm or 1550nm.

The wavelength currently widely used in automotive LiDAR is 905 nm. In fact, 905 nm LiDAR systems can be built using off-the-shelf components (high power edge emitting pulsed diode lasers and detectors based on silicon photodiodes or photodiode arrays), therefore, reducing cost. This reduction in cost can be attributed to the compatibility with 905 nm CMOS detector arrays [49] and the implementation of optical phased array technology [60].

However, 905 nm LiDAR range is limited (i.e. ~100 m), mainly due to the limitations placed on the maximum power used in the laser pulses at this wavelength for eye-safety. For the human eye, a maximum permissible exposure (MPE) has been defined, and it corresponds to the highest optical energy density (in J/cm^2) considered safe (not harmful) for a fixed time of exposure and a specific wavelength. The longer the exposure, the lower the allowed power. With the same exposure time, the MPE for 905 nm light sources is 2-3 orders of magnitude lower than for 1550 nm, meaning that 1550 nm LiDAR can use higher power with minimized risk to the human eye [61]-[63]. Eye safety is one of the main reasons behind the proposal of 1550 nm as emerging alternative for automotive LiDAR; higher permissible optical power correlates to better performance (higher signal to noise ratio, increased robustness to noise factors) and increased R_{max} [64]. Nonetheless, the potential enhanced range must be balanced with the increased power consumption. Furthermore, 1550nm LiDAR production cost in comparison to more traditional wavelengths could be higher. This higher cost can be attributed to two factors: the use of more exotic materials for the components, such as indium phosphide emitters [65]; key components not available through standard supply chains. However, 1550 nm is a mature technology for telecommunication applications and due to the remarkable progress of Silicon Photonics in the last few years, particularly in terms of cheaper receivers (e.g. CMOS compatible devices, based on Silicon Germanium or on Silicon defect-mediated photodetectors), the cost factor is projected to decrease remarkably in the near future [66]-[68].

Adverse weather is a challenging situation for most of the sensor technologies (Fig. 4). It is paramount that the impact on perception sensors from different weather types is mitigated. Fog can have a significant impact on 905 nm LiDAR, as LiDAR beam can be scattered by the fog. The scattering results in a decreased sensing range, in addition to the appearance of artifacts and false positives [64], [69]-[70]. Various recent studies have investigated the effect of weather on different wavelengths of LiDAR, particularly of rain and fog. The effect on both wavelengths is similar, as at the same optical power there is a small difference (<10%) between the two [71]-[72].

Overall, it can be said that 1550 nm is a superior wavelength to 905 nm due to an increased allowed optical power, resulting in a higher range and slightly diminished impact of adverse weather. However, in power critical and cost critical applications, such as automotive, it can be said that 905 nm wavelength is suitable until the cost of 1550 nm LiDAR is reduced and the battery technology in autonomous vehicles increases further so the power required is not as impactful.

B. Scanning LiDAR

In Fig. 3, we have divided LiDAR technologies into two big categories that are able to generate a 3D pointcloud of the vehicle surroundings, namely 'scanning' and 'non scanning'. In this subsection we will focus on scanning LiDARs, entailing some techniques to rotate the laser beams and therefore covering the sensor FoV (optical techniques will be thoroughly covered in sections IV-V), in the following subsection we will focus on non scanning LiDAR.

Mechanical Rotation

LiDARs with 360° HFoV seen in automotive, like Velodyne HDL-64E, generally work by revolving the optical components (lasers and detectors) around the vertical axis. To cover the VFoV multiple emitters/detectors are piled and aligned with rotation axis (increasing the size of the device), Fig. 5. The obvious advantage of these devices is that a single sensor is able to cover front, back and side views around the ego-vehicle [73]. However, 360° LiDAR usually has a large sensor unit that needs to be mounted on the vehicle roof, resulting in it being an extremely unaesthetic and impractical solution for production vehicles.

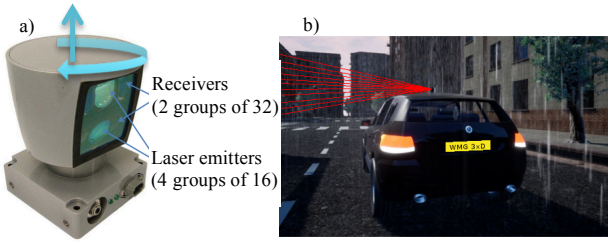

Fig. 5, (a) Mechanical Rotating LiDAR, modified from [74]; (b) 360° rotating LiDAR on a vehicle, red lines represent the vertical channels

Another option for mechanically rotating LiDARs is to have rotating mirrors and fixed sources/detectors, and again multiple optical components along the vertical axis. In this case, HFoV is limited to around 100° [56]. In both cases, the density of the pointcloud on the horizontal axis will depend on the rate of emissions per optical device and how fast the optical column is rotating, and on the vertical axis on how many optical devices are there. Rotating mechanisms are usually limited in terms of speed and they are power hungry, as they need to counteract the inertia of the rotating module (e.g. Velodyne HDL-64E weights almost 13 Kg). Overall, this type of LiDAR is bulky and heavy, very expensive, and reliability is questionable as mechanical parts wear out, and even small misalignments can affect optical performance. In the automotive environment, these misalignments can be easily caused by shocks, jolts and vibrations.

Other Rotation Mechanisms

Although mechanical LiDAR has initially dominated the field of LiDAR for automotive, its prohibitive cost and its bulkiness have promoted the development and testing of novel

solutions. One promising alternative to macro-mechanical rotation, it is to look into micro-mechanical rotation using micro-mirrors integrated on silicon chips, in other words leveraging the mature micro-electro mechanical system (MEMS) technology (used in consumer electronics, e.g. inkjet printers, as well as aerospace and robotics). In this case, the size of miniaturized suspended mirrors on silicon chips is of few mm squared; therefore they offer the possibility to overcome the bulkiness of macro-mechanical rotating LiDAR. Furthermore, MEMS processing is offered by mainstream Silicon foundries, therefore large-scale and low-cost solutions are achievable.

These micro-mirrors used to steer the LiDAR EM beam can usually change their inclination along 2 different rotation axes and therefore can scan the HFoV and VFoV [75]-[78]. In this case, a 360° HFoV is not achievable, but devices with performance that are compatible with the automotive environment are on the market (e.g. InnovizOne, 115°x25° HFoV x VFoV [79]). Moreover, by using multiple channels and fusing their data allows the creation of pointclouds with enhanced densities with respect to macro-mechanical LiDARs [80]-[81]. The MEMS mirrors require to be specifically designed for automotive LiDAR applications, for example, there is a trade-off between device miniaturization and maximum detection range (the mirror needs to be big enough to collect sufficient light reflected by the target) [82]. More information of different ways of implementing a laser scanner using MEMS mirrors is given in [83] and is outside the aim of this paper.

There are some MEMS LiDAR companies currently working with automotive OEMs, such as Innoviz and Innoluce [79], [84], as this technology offers compact and low weight devices, low cost for high volume of manufacturing, compatibility with microelectronics processes and low power consumption; all of these factors are a remarkable advantage with respect to LiDARs based on macro-mechanical scanning.

C. Non scanning LiDAR

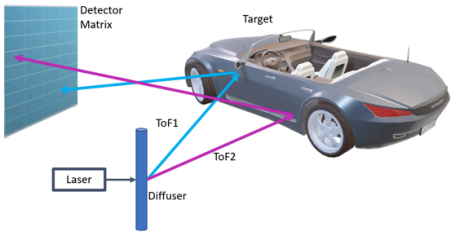

Fig. 6, Schematic representation of the ToF principle applied with the detector array in a Flash LiDAR.

The most common technology for non scanning LiDAR in automotive is Flash LiDAR; flash sensors do not have any rotating components and therefore promise to be more robust and less prone to mechanical wear out. This technology has evolved in the last few years, and there are some solutions for short medium range almost ready for commercialization. Unlike scanning LiDARs, FLASH LiDAR generates an electromagnetic pulse (usually in the near infrared, NIR) that floods completely the sensor field of view and detection range [73]. Each object in the covered detection volume will reflect the emitted beam, and the LiDAR unit will detect reflected light on an array of pixels, designed to detect light in the wavelength range of the emitted pulse [85]. Usually in Flash LiDAR the beam is diffused, to make sure that the detection volume is covered almost uniformly by the emitted EM beam.

Due to the spatial position of the different objects in the detection volume, the reflected light will travel back to the pixel array with slightly different ToF. As a consequence, the LiDAR can measure the distance of each object by measuring the received signal ToF for each pixel, as schematically shown in Fig 6. As a result, the outputs of these sensors include distance, location on the pixel array, and reflected intensity of the detected objects. Differing from scanning-mechanic 3D LiDARs, it captures the information into an image. Therefore, the lack of moving parts, fast frame rates and the packed data in a single image lead to efficient and reliable data [86]. However, the detectors are way more complex and expensive (standard CMOS detectors used for visible light cannot be used for NIR) with respect to detectors used in scanning LiDARs. Furthermore, they are limited to short/middle range due to concerns around maximum power emitted, hacking and saturation risk, wavelength and eye-safety. In addition, flash LiDAR performance depends on the reflectivity of objects.

IV. ALL OPTICAL LIDAR

While microelectronics is facing its ultimate limits [87], Silicon Photonics (SiPho) is emerging as an enabling technology in several fields, from telecommunications to interconnects, from biomedicine to sensing [88]-[90]. Silicon Photonics is based on a combination of photon manipulation and miniaturized optical components integrated onto silicon chips (Silicon on Insulator, SOI, chips), to guide and direct the EM radiation with low loss and high performance. SiPho started as a platform for telecommunications, but rapidly evolved to offer signal filtering, routing, modulation (at 50 GHz and beyond), and photo detection (using silicon defects or silicon germanium [67]-[68]). All of the most advanced silicon foundries in the world have currently some SiPho offerings. Foundry compatibility is one of the SiPho greatest advantages, as it enables low cost and high-volume production of sensors with extremely small footprints, as required by the automotive industry [91]-[94].

A. Optical Phased Array based LiDAR

The idea of steering EM beams and controlling their direction using phase delay and interference between several transmitting antennas was firstly used for RADIO waves [95]. Even though LiDAR wavelengths are different with respect to RADIO waves, the working principle is exactly the same, and optical phased arrays (OPA) have been recently proposed as a promising solid state technology to achieve fully integrated and cheap LiDAR sensors on SiPho chips [96]-[99]. The concept of integrated OPA for NIR light was well known before, as it was presented, based on AlGaAs waveguides, in the early 90s [100]; however, it is now gaining more momentum, driven by the automotive market. The AlGaAs OPA was a first attempt to achieve limited beam rotations (of the order of few mrad, ±7.2 mrad, at λ=850-900nm), but due to the materials/components used it was still too big to be

integrated in a cost-effective way on chip (the emitting antennas had a footprint of the order of more than 10 mm^2). The key challenges to achieve a competitive SiPho OPA LiDAR are: achieving an efficient beam steering into two dimensions, to collect a dense 3D pointcloud; achieving enough output power to reach medium to long range; power consumption; laser integration and integration with driving electronics (par. V.C-V.D); thermal stability (par. V.E); real-time processing of the data. We will discuss in detail some of these aspects in the remaining parts of this section.

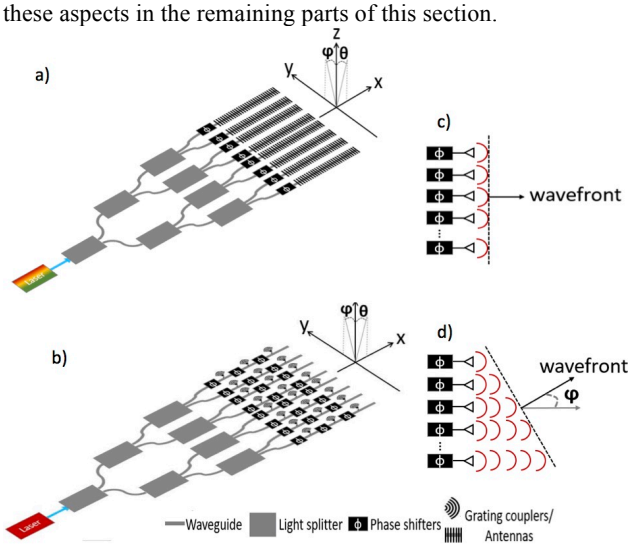

Fig. 7, Schematic representations of: the transmitting components and the emitted beam angles φ and θ in a 1D-OPA (a) and 2D-OPA (b) based LiDAR; the emitted waves with no phase delay between the emitting elements (c), and with phase delay (d), causing a rotation of the emitted wavefront along φ.

B. OPA-LiDAR components

As schematically illustrated in Fig. 7a-b, an integrated silicon photonics OPA-LiDAR consists of several parts: the light source; a device (usually an MMI or a star coupler [99], [101]-[102]) used to split the beam into the several emitting elements; phase shifters (thermal or electro-optical), to introduce different phase delays to the signals in the antennas, and therefore to achieve the steering of the emitted beam into a specific direction (Fig. 7c-d); the antennas themselves, usually in the form of gratings or edge or end-fire couplers [103]-[104]. In terms of antennas, we will focus only on the former type (based on grating couplers, GCs), as edge emitter have been demonstrated only for 1D steering, whereas in automotive 2D steering is needed to achieve a suitable 3D pointcloud. In OPA-LiDAR, 2D steering can be implemented in two ways: (i) a 1D array of GCs, where steering in the longitudinal direction, θ, is achieved via tuning the laser wavelength, and in the lateral direction, φ, by the phase delay, ϕ, between the light injected in each GC (Fig.7a); (ii) via 2D matrixes of GCs, and in this case the phase delay between the elements in the matrix creates the steering in the two directions (Fig.7b). The backreflected signal will need to be received via a photodetector, and then post-processed to extract the relevant information (ToF, intensity, etc.), but these steps are outside the aim of this paper. All of the above mentioned components have a key role in the final performance of the SiPho LiDAR; hereafter we will focus on the emitting elements as a combination of the phase shifters with the antennas based on gratings. In terms of SiPho LiDAR components, there are two main technological choices, using Si as light conducting material or SiN (as shown also in Table II), some advantages and disadvantages of these two options are described in par. V.A.

Phase Shifters

On Silicon Photonics chips, phase shift has been mainly implemented using two different methods of varying the refractive index of the silicon waveguide (and therefore the speed of the light propagating through the waveguide):

- *thermo-optic (TO) effect*: the refractive index of materials depends on the temperature; for Silicon, it has been measured that the variation of the refractive index, n_{Si}, is $dn_{Si}/dT = 1.87*10^{-4}$ K^{-1}, for wavelengths around 1500 nm and temperature nearby T= 295K [105]. Silicon waveguides can be made hotter by using the descending heat of a metal layer deposited on the top of the upper cladding (Fig. 8a); the metal layer will warm up from the Joule effect when a voltage is applied to it. As a consequence, the n_{Si} will change, introducing a phase delay with respect to a waveguide of the same length not heated up. Commonly used SiPho thermo-optic phase shifters have power consumptions on the order of 15 mW/π. TO phase shifters implemented with metal heater have the advantage of introducing almost no loss to the signal, but usually operates at a lower speed [106]-[107].
- *electro-optic (EO) effect*: in this case the change in n_{Si} is achieved by charge-injection, due to the creation (and actuation) of a p-i-n structure along the transverse section of a rib waveguide (p and n dopants are added to each of the lateral sides of the waveguide, Fig. 8b). Similar to TO effect, the variation of refractive index will introduce a delay with respect to the not doped/actuated waveguide. In this case, high-speed beam steering can be achieved (with a nanosecond switching speed), but the dopants increase the waveguide loss and the design is more complicated. Some of the proposed injection-based phase shifters require 10 mA/π, but generally they have lower power consumption with respect to TO. EO p-i-n phase shifters offer higher speed operation with respect to TO ones, but they have variable insertion loss [107]-[109].

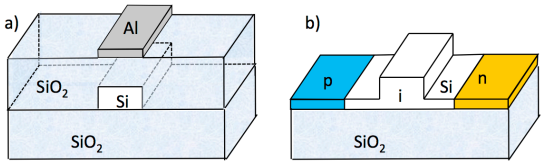

Fig. 8, Schematic representation (not at scale) of the structure cross-section of (a) a TO phase shifter with Silicon strip waveguide, SiO_2 lower and upper cladding, and heater metal layer (Aluminum or other metals compatible with CMOS thin layer deposition); (b) EO phase shifter with Silicon rib waveguide and doped (p and n) waveguide sides, SiO_2 lower cladding; upper cladding not represented. In both of the structures the metal layer or doped sides need to be actuated.

Optical Phased Array parameters

The OPA is an array of antennas or emitting components (to the aim of this paper GCs, Fig.7a-b) that are designed to enhance the NIR light emission and beam steering. There are several design parameters that can be used to optimize GC

interference in order to enhance the OPA performance in terms of maximum steering (along two axes), beam directionality, suppression of side lobes and reduction of crosstalk, emitted power. In Table II, we have summarized some of these design parameters along with beam key performance indicators (KPIs), as discussed below, for 26 SiPho OPAs proposed in the last 11 years [98]-[99], [101], [104], [110]-[131]. It is worth noting that also the design of the phase delay will contribute to the OPA final performance.

- Array size: this value is given as '*antenna elements on the longitudinal axis (M)* x *elements on the lateral axis (N)*', (leftmost column, Table II). MxN represents the total number of GCs in the OPA, and therefore how many signals are combined to steer the emitted beam in the far field. If one of the two numbers in this column is '1' (e.g. 1x16) the array is a 1D array, and GC signals are combined to steer the beam usually along the lateral direction, φ; otherwise, the array is a 2D array. In the Table II, the last row has only one value in this box, this OPA is a 2D array of elements with non uniform distribution, and 2D steering can be achieved [131].
- Element spacing, d (μm): this value represents the distance of GCs in the array. Combined with the array size above gives an approximation of the total antenna footprint.
- Wavelength, λ_0, and wavelength range $\Delta\lambda$ (nm): λ_0 expresses the central wavelength the GC has been designed for. Some 1D arrays are designed to steer the emitted beam along the second direction (usually the longitudinal direction, θ) by varying the injected wavelength in the antennas, typically in a range nearby the central wavelength ($\Delta\lambda$).
- Lateral steering range, φ_{max} (^{o}): it represents the lateral FoV. It can be calculated using Eq. 5, where ϕ is the uniform phase difference between the signals emitted by the GCs [110].

$$sin\varphi_{max} = \frac{\lambda_0 \phi}{2\pi d} \quad (5)$$

As known in radio waves OPA theory, to avoid the presence of the so-called '*grating side lobes*' (lateral, unwanted lobes) in the emitted beam, d should be smaller than $\lambda_0/2$ [132]. These small spacing increases the design complexity, as cross talk between the GCs needs to be minimized. In equally spaced GCs with the same phase delay introduced in all the elements (e.g. $\phi=0^o$ for all the GCs), the angular position of these undesired grating side lobes limits the maximum achievable steering range (see also following point).

- Lateral beam width, $\Delta\psi_{FWHM}$ (^{o}): it represents the width of the beam in the later direction. The smaller this indicator, the more directive is the generated beam [110], [132].

$$\Delta\varphi_{FWHM} = \frac{0.886\lambda_0}{Ndcos\varphi} \quad (6)$$

The beam width depends on the aperture size of the OPA (Nd), the larger the aperture size the narrower is the beam. However, increasing the aperture size while maintaining the same number of antenna elements results in augmented element spacing and reduction of the lateral FoV, therefore there is a design trade-off to optimize these values [120]. Conversely, the closer the waveguides (i.e. smaller d) the higher their crosstalk will be; augmented crosstalk can increase the power losses, and decrease the power efficiency. Having a highly directional beam improves the lateral resolution of the sensor, particularly in the medium-long range. In fact, an angular resolution around 0.1° is required for distinguishing any potential hazards (and vulnerable road users, such as pedestrians) even at a distance of 200 m. A 0.1° beam divergence at wavelength 1550 nm corresponds to an aperture size of 1.13 mm. One approach to keep the beam width narrow and the OPA design compact is the use of arrays with non-uniform GC distribution [131]; the non-uniform distribution of the elements enables a wide steering range and suppression of the 'grating side lobes' (see point above) [133]. Two designs are worth mentioning in terms of excellent achieved lateral beam width: 0.02° beam width has been achived in 2016 using SiN waveguides [101], and in 2018 Chung et al. have proposed a similar design in silicon waveguides achieving a beam width of 0.03° [126].

- Longitudinal steering range, θ_{max} (^{o}): the longitudinal FoV can be controlled in 2 ways: the first one is to have multiple GCs in the longitudinal direction, Fig. 7b (in this case Eq. 5 can be used substituting φ with θ, and d will be the GC distance along the longitudinal axis), [116]; the second one is controlled by tuning the wavelength injected into the antennas (represented in Fig. 7a) [104]. In this case, the emission angle can be calculated based on Eq. 7, where Λ is the grating period, n_{eff} is the effective index of the waveguide at λ_0, n_{clad} is the refractive index of the cladding material, surrounding the Silicon waveguide core, (e.g. n_{clad} is n_{SiO2} in Fig.8a). It worth noting that n_{eff} is a function of temperature and wavelength [107].

$$sin\theta_{max} = \frac{\Lambda n_{eff} - \lambda_0}{\Lambda n_{clad}} \quad (7)$$

With an average wavelength steering of about 0.15^o/nm (Table II), and a typical VFoV for automotive LiDAR of ~20^o -25^o, a $\Delta\lambda$ of 100nm to 200nm is needed, establishing a stringent requirement on the LASER source.

- Longitudinal beam width, $\Delta\theta_{FWHM}$ (^{o}): similar to the lateral beam width, it represents how wide the beam is in the longitudinal direction. If the rotation along this direction is caused by the combination of multiple elements along the longitudinal axis, the beam width can be calculated by suitably modifying Eq. 6; otherwise, it will depend on the grating structure, its length, and selected wavelength.
- Power Consumption: this value quantifies power consumption per antenna in mW per π-shift. Even though the reviewed structures are different and some of them have limited performance, this value gives an indication of the potential to use these structures, in automotive LiDAR in an energy efficient way. Most of the proposed OPAs have power consumption of around 10 mW/π, but there are some more power hungry structures with about an order of magnitude higher consumption [99], [112]-[113], [115], [121], [129].
- Achievable range (not in Table II): this important LiDAR KPI is not always discussed into published works, but 200 m range is reported in [104], and 150 m in [134].
- Other design parameters (not in Table II). In the above points, we have mentioned several times the OPA aperture size, (Nd), and the element spacing, d, as key deign parameters. Moreover, the maximum achievable *OPA gain* is

TABLE II
DESIGN PARAMETERS AND KEY PERFORMANCE INDICATORS (PAR. IV.B) OF PUBLISHED SIPHO PHASED ARRAY.

Design Parameters			Key Performance Indicators						
Array size (MxN)	d (μm)	λ_0, $\Delta\lambda$ (nm)	φ_{max} (°)	$\Delta\varphi_{FWHM}$ (°)	θ_{max} (°)	$\Delta\theta_{FWHM}$ (°)	Power (mW/π)	Year	Ref., notes
1X16	2	1550 1500-1600	2.3	2.7	14 (0.14°/nm)	2.5	8	2009	[110] First Si photonics OPA
1X12	Non-uni.	1550	31.9	1.7	-	-	12	2011	[111]
1X16	5	1550	23	1.27	-	-	97	2011	[112]
1X16	3.5	1555, 1525-1625	20	0.6	14 (0.14°/nm)	1.6	215	2011	[113]
1X16	2	- 1500-1600	50	3.5-4	15 (0.15°/nm)	3.5-4	-	2011	[114]
1X8	5.5	1594	12	1.8	-	-	97	2012	[115] First on chip laser
1X8	5.5	1539	16	0.16	(0.14°/nm)	-	40	2013	[98]
8X8	9	1550	9.9	1.1	-	-	8.5	2013	[116] 2D array
8X8	9	1550	12	1.6	-	-	8.5	2014	[117]
1X16	4	1550, 1480-1580	20	1.2	15 (0.15°/nm)	0.5	20	2014	[118]
1X16	2	1550	51	3.3	-	-	13	2014	[119]
2X2	4	1550	30	-	-	-	-	2015	[120]
1X32	4	1580, 1555-1605	23	1	3.6 (0.07°/nm)	0.6	160	2015	[121]
4X4	18	1550	4.93	2	-	-	-	2015	[122]
8X8	33	1550	1.6	0.45	-	-	14.2	2015	[123]
4X4	50	1550	1.8	0.5	-	-	-	2015	[124] First charge injection
1X50	2	1550, 1454-1641	46	0.85	36 (0.19°/nm)	0.18	13	2016	[125]
1X128	Non-uni.	1300, 1260-1360	80	0.14± 0.02	17 (0.17°/nm)	0.142± 0.005	80	2016	[99]
1X1024	4	1550	-	0.02	-	-	-	2016	[101] SiN waveguide
1X1024	2	1550	45	0.03	-	-	54	2018	[126]
1X512	1.3	- Δ=45	70	0.15	14 (0.3°/nm)	0.15	2.6	2018	[127]
1X512	1.65	1550, 1450-1640	56	0.04	15	-	<1	2019	[104] lowest power consumption
1X24	1.3	1550, 1540-1560	> 40	-	3.3 (0.165°/nm)	-	-	2019	[128] SiN waveguide
1X4	3	905	17.6	4.3	-	-	88	2019	[129] SiN waveguide
1X16	0.8	1550	64	6.7	-	-	-	2019	[130]
128	Non-uni.	1550	16	0.8	16	0.8	10.6	2019	[131] 2D non-uni.

proportional to $2Nd/\lambda_0$, therefore decreasing element spacing will affect also the maximum emitted power and, as a consequence, the achievable range.

V. DISCUSSION AND PERSPECTIVE

In the last ten years, the research in the field of OPA-LiDAR has been gaining more and more interest, and some of the reviewed works have been the starting point for the creation of new startups (e.g. [58], [135]-[136]). However, there are several design tradeoffs and challenges in designing SiPho OPAs, (e.g. the achievement of compact structures, with packed and highly efficient elements vs. sensor resolution and range), and some novel solutions have to be explored to ensure this technology can meet and exceed the automotive requirements. Here, we will cover some of the current design challenges and opportunities.

A. Silicon versus Silicon Nitride

Integrated optical waveguides in the near infrared range can be fabricated using silicon or silicon nitride (SiN) cores, and both of these materials are compatible with foundry processes. Both technologies have been used to demonstrate OPA LiDARs with competitive performance (e.g. [101], [128]-[129]). SiN offers the possibility to be transparent over a wider range of wavelengths, including shorter wavelengths and 905 nm. As a consequence, 905 nm know-how and off the shelf components can be used in combination with SiN waveguides to build solid state LiDARs. Moreover, SiN waveguides can stand higher optical power with respect to Si ones. In fact, typical foundry compatible Si waveguides (220 nm thick) work linearly with powers of the order of few hundreds mW; above this range nonlinear effects start to arise. However, Silicon based waveguides allow for smaller footprints, in terms of waveguide dimensions and bending radii. Si waveguides can have smaller bending radii (as small as 5 μm radii) without increasing notably the propagation losses; on the contrary, SiN waveguides need to have bends with radii in excess of 20 μm. Finally, phase-shift can be implemented in Si using EO and TO effects, whereas in SiN the TO efficiency has about one order of magnitude lower power efficiency than in Si [137]-[138]. Recent works have also proposed highly customizable photonics processes, where Si and SiN elements can be combined to achieve optimized beam steering [139].

B. Grating coupler design

In par. IV.B, we have discussed in details OPA performance and mentioned that it depends also on the selected GC design. GCs are widely used SiPho components, and in OPAs they are used as the elements that emit the NIR light outside the waveguide to create the directional LiDAR beam [137]-[138], [140]. Several different designs have been proposed to achieve this radiation with low losses; ideally, after the phase shifters, all the light propagating into the waveguides should be emitted. As represented in Fig. 9, the two most common waveguide based GC designs are the side modulated gratings (basically the waveguide width switches between two values with a defined duty cycle and period), and the shallow or deep etched grating (in this case the foundry Si etches are used to have the waveguide height switching between two values with a defined duty cycle and period), [99]. Another promising approach is to use shorter GCs with strong perturbations (e.g. fully etched gratings), leading to compact structures, as demonstrated in [116]. However, many different designs have been proposed to implement gratings on SOI chips, for example by modulating the refractive index of the cladding, or by using sub-wavelengths gratings (SWG) or multi-box SWG to engineer the effective index of SiPho waveguides and sensors [89]-[90], [141]. SWG-based sensors offer enhanced performance with respect to similar sensors based on regular waveguides; this enhancement is due to NIR light propagation in SWG waveguides with low loss but increased evanescent field. By tuning SWG parameters (period, duty cycle, materials, structures) and grating parameters, it can be possible to engineer optimized GCs for LiDAR applications. Conversely, grating structures have great variability in fabrication and this variability can affect their performance; furthermore, depending on the specific design they might be not compatible with CMOS processes due to very small features required. Fabrication variability represents a remarkable issue that needs to be addressed by SiPho technology if automotive reliability and robustness standards have to be met.

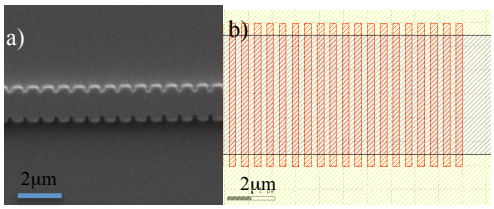

Fig. 9, (a) SEM picture (top view) of a side modulated grating waveguide on SOI chip; (b) layout of an etched grating waveguide on SOI chip, where the red lines represent a partial etch (70 nm deep) of the Si layer, 220 nm thick. The two black lines delimit the waveguide.

Two main challenges related to GC design still need to be properly addressed to improve current light steering on chip:

1. *making longer antennas with uniform and unidirectional emission.* Longer GCs are desired, as increased GC length means decreased longitudinal beam width ($\Delta\theta_{FWHM}$), and therefore enhanced beam directionality [142]. However, uniform perturbation strength and long GC structures present a decaying emission along the grating length [140]. One well-known solution to counteract the decaying emission is to tailor the grating perturbation strength in the propagation direction using apodized gratings. An enhanced and uniform grating emission is ideal to maximize GC effective aperture size that is critical for both OPA gain and beam width (par. IV.B). The beam uniformity depends also on GC field emitted towards the chip substrate and then reflected back upwards. Specific designs to mitigate these reflections have been proposed, e.g. GC based on multiple emitting layers, or with buried reflectors [140], [143].
2. *reducing the grating side lobes to increase the lateral FoV.* It is well known from Radio Frequency waves that uniformly spaced antenna arrays need to have element spacing such as $d < \lambda_0/2$. If this condition is fulfilled, grating side lobes are dramatically reduced, and it is possible to use the main lobe to sweep the entire FoV. However, in integrated photonic devices, distancing parallel long waveguide based devices is needed to avoid unwanted coupling between these antenna elements [144]. There are several design choices than can help in inhibiting the side lobes, and we will mention here the most common ones. Non-uniform and/or aperiodic arrays have been recently studied specifically for suppression of side lobes. However, the spacing of the components was bigger than λ_0, therefore this approach can suppress side lobes, but increases device footprint without increasing the number of emitting elements [133]. Conversely, in 2019, subwavelength pitch arrays have been demonstrated with more than 40° lateral beam steering, no grating side lobes in a FoV of about ± 33° [129]. Another proposed way of reducing grating side lobes is to optimize the phase delays between the array elements, instead of using uniform phase delay [145].

C. Light source integration

One important aspect for SiPho LiDAR is the integration of the light source on SOI chips. This aspect represents one of the biggest challenges for SiPho. Some solutions have been proposed, but they are not mature or cost effective; an optimized design is still under investigation [146].

Despite laser integration challenges, during the last decade, many works have demonstrated optical beam steering and light source integration on chip by using hybrid III/V silicon technology [115], [121], by using InP technology [147], or via integration with rare-earth doped glass sources [148].

The first demonstration of 1D beam steering with integrated laser source was shown in 2012 [115]. In this case, a single wavelength laser was combined with eight grating couplers to achieve 12° lateral FoV. Building on previous works, in [121], Hulme et al. combined a 2D beam steering with two different III-V laser designs, the performance of the related OPA are reported in Table II. A similar design approach is reported in [147], however the Authors selected InP based photonic integrated circuits, as tunable lasers are available using this platform. Furthermore, InP is a mature photonic technology, and offers integrated semiconductor optical amplifiers (SOAs) to boost the optical power, and InP phased shifters with up to GHz bandwidth. Recently, an electronically steerable silicon photonic OPA has been monolithically integrated for the first time with a rare-earth-doped laser, pawing the way to meet the power budget requirements for OPA-LiDAR [148].

Three main laser parameters are crucially important to the

aim of OPA-LiDAR performance: tunability, spectral linewidth and emitted power. Tunability is particularly important for 1D CG arrays, as in this design, the steering along θ is achieved by tuning the laser wavelength (Table II, Fig.7a). Therefore, the smallest change in emitted wavelength that can be transformed into a change of emitted θ, the better will be the LiDAR resolution against the longitudinal emission. Similarly, the spectral linewidth represents the laser spectral density width, and it is key for the resolution along the two direction of emission, along with the spatial beam widths defined in par. IV.B. Finally, emitted laser power, combined with a low loss photonic circuit, is fundamental for maximizing the LiDAR maximum range.

Some recent works have been focusing on heterogeneously integrated tunable laser sources for many applications, including integrated LiDAR [149]-[151]. The tuning of the emitted wavelength can be achieved by using microring resonators in a Vernier configuration, as shown in [149]-[150]. In [149], the authors demonstrated a laser tuning range of 46 nm (1527 nm-1573 nm), achieved by thermally tuning the Vernier rings, with up to 1.6 mW output lasing power. The proposed solution has a laser linewidth of 340 kHz, moreover, the laser output can be further stabilised to make it particularly suitable for OPA-LiDAR. Besides, Tran et al. demonstrated a heterogeneously integrated laser combining the Vernier resonators with a Mach-Zender Interferometer. The proposed laser achieved enhanced performance with 55 nm tuning range and a narrower linewidth (50-85 KHz), with a maximum output power of 8.5 mW [150].

D. Integration with driving electronics

Another key challenge for SiPho is the integration of the photonic circuitry with the driving electronics, either through heterogeneous or monolithic integration. This aspect is pivotal for OPA-LiDAR as well, as electric signals will be used to drive it and will be needed as sensor output; for this reason, in the last few years, several works have been focusing on combining on a single chip all the LiDAR electronics and photonics components [126], [131], [139], [152]. Monolithic integration is one of the techniques that can combine electronics and photonics [126], however CMOS design rules limits the photonics circuit design and ultimately the OPA performance. Chung et al. proposed a scalable architecture for SiPho optical beam steering monolithically integrated on the same wafer (without modifying the SOI platform) with a 180 nm CMOS electronic driving circuit [126]. In [131] a very compact design of the integrated OPA and beam steering photonics circuit (2.08 mm^2) and its driving electronics (1.7 mm^2) is presented; they are fabricated respectively via a SOI process and a 65-nm CMOS process. Heterogeneous integration allows for the independent optimization and tailoring of the CMOS and the photonic processes, enabling more flexibility in the design. A promising solution to achieve seamless heterogeneous integration is to use 3-D integration platforms, to optimize the two processes separately, and then combine them, e.g. using oxide bonding [139], [152].

E. OPA and thermal management

In par IV.B we have discussed how silicon thermo-optic effect can be leveraged to achieve TO phase shifter. However, this effect can affect the performance of the optical devices, particularly in phase-sensitive application such as OPA LiDARs and their beam steering. Even small variations in the chip temperature can modify the phase delay between the signals in the emitting elements, and therefore degrade OPA performance. This aspect has been reported in [126], describing that temperature variation can disturb steering accuracy, grating side lobe suppression and beam width.

Temperature variations on SiPho chips can be caused by poor heat dissipation, overheating of some components, or by temperature gradients due to packed on-chip components. For these reasons, thermal management solutions, compatible with SiPho and CMOS processing, are crucial for the achievement of OPA-LiDAR. Two approaches have been recently proposed and evaluated specifically to improve thermal management on SiPho chips with phase-sensitive components [153]: the first solution is based on using deep trenches (etching down all the buried oxide layer and partially the silicon substrate) to separate different thermal regions in the photonic integrated chip; the second solution uses heat shunts to transport heat far from delicate photonic components. We expect that, thermal management strategies will be a crucial element for achieving stable and robust OPA-LiDARs.

F. OPA comparison with other LiDAR technologies

In this paper, we have reviewed some of the proposed and emerging technologies available for automotive LiDAR; in Table III, we compare them with OPA-based LIDAR. This comparison is based on a similar qualitative evaluation presented in [57] combined with our experience with automotive LiDARs. Most of the drawbacks of other technologies that have been previously discussed are highlighted in the table, such as: *rotating LiDARs* have currently the best performance in terms of R_{max} and FoV, however they are bulky, expensive, and they easily wear out, therefore their robustness and lifespan are unsatisfactory; *MEMS-LiDARs* offer decreased R_{max} and FoV with respect to rotating solutions, however they are compact and promise increased robustness and lower cost for large scale production; *Flash-LiDARs* have the advantage of not having rotating mechanisms, but they are dramatically limited in range and FoV, and complex on the detection side. It is worth noting that despite technology readiness for OPA-LiDAR is the lowest, as most of the components need further optimization for the specific application, its potential is very high. In fact, OPA-based LiDAR components are miniaturized, inherently immune to EM interference, and compatible with foundry processing. On this note, Rahim et al. have recently reviewed SiPho platforms (focusing on European platforms), discussing several aspects including their technology readiness levels (TRLs) and applications these foundries can support [147]. Several of the discussed platforms offer processes that can support integrated OPA-LiDAR fabrication and have TRL of 5 and above (TRL5 means that the fabrication process flow has been "successfully developed in an environment with manufacturing-grade tools or wafer-level prototyping tools" [154]). Amongst them, it is worth noting LIGENTEC [155], an open-access foundry,

particularly focused on high-power LiDAR as one of their main applications, and based on nitride-core technology. In [154], LIGENTEC is recognised as able to achieve TRL 8-9.

OPA-based LiDAR can offer in the near future the solution to most of the drawbacks of current LiDAR devices used in automotive, and discussed in par. II.F and section III.

TABLE III
PERFORMANCE COMPARISON OF LIDAR TECHNOLOGIES, MODIFIED FROM [57]; '++' VERY GOOD, '+' GOOD, '0'NEUTRAL, '-' UNSATISFACTORY.

	Rotating	MEMS	OPA	3D Flash
R_{max}	++	+	+	-
FoV	++	+	0	0
Signal-to-Noise Ratio	+	+	++	0
Module Size	-	+	++	+
Robustness	-	+	++	++
Unit Price: 2019	-	0	0	0
Target Price: 2030	0	+	+	+
Product Lifetime	-	+	+	+
Technology Readiness	+	0	-	0

VI. CONCLUSION

We have discussed the fundamental role of LiDAR as an enabler for safe and robust automated vehicles, and as a strong candidate to complement the other sensor technologies. Affirmation of LiDAR is hindered by its bulkiness and expensiveness, but novel solutions, such as optical phased array LiDAR can overcome these issues. We reviewed and discussed OPA-based LiDAR advantages and disadvantages, looking into possible evolutions of this promising technology.

REFERENCES

[1] SAE International, *Taxonomy and Definitions for Terms Related to On-Road Motor Vehicle Automated Driving Systems*, SAE J3016™, 2018.

[2] C. Bolstad, H., Cuevas, J. Wang-Costello, M. Endsley, and L. Angell. "Measurement of situation awareness for automobile technologies of the future," *Performance metrics for assessing driver distraction: the quest for improved road safety*, pp.195-213, 2010.

[3] W. Elmenreich, *An introduction to sensor fusion*, Institut fur Technische Informatik, Technischen Universitat Wien, 2002. Accessed on: Apr. 13, 2020. [Online]. Available: https://www.academia.edu/649942/An_introduction_to_sensor_fusion.

[4] W. Daimler, *Reliable environment perception also in adverse visibility conditions*, Dense247.eu, 2019. Accessed on: Apr. 13, 2020. [Online]. Available: https://dense247.eu/fileadmin/user_upload/PDF/1707_DENSE_A4_factsheet_v0.11.pdf.

[5] *Ground Plane and Obstacle Detection Using Lidar*, The MathWorks Inc.. Accessed on: Apr. 13, 2020. [Online]. Available: https://uk.mathworks.com/help/releases/R2017b/driving/examples/ground-plane-and-obstacle-detection-using-lidar.html?searchHighlight=lidar&s_tid=doc_srchtitle.

[6] A. Polychronopoulos, M. Tsogas, A. J. Amditis and L. Andreone, "Sensor Fusion for Predicting Vehicles' Path for Collision Avoidance Systems," *IEEE Transactions on Intelligent Transportation Systems*, vol. 8, no. 3, pp. 549-562, Sept. 2007.

[7] W. Ritter, M. Bijelic, T. Gruber, M. Kutila, and H. Holzhüter, "DENSE: Environment Perception in Bad Weather—First Results," *Springer Electronic Components and Systems for Automotive Applications*, pp. 143-159, 2019.

[8] P. H. Chan, G. Dhadyalla, and V. Donzella, "A Framework to Analyze Noise Factors of Automotive Perception Sensors," in *IEEE Sensors Letters*, vol. 4, no. 6, pp. 1-4, June 2020, Art no. 6001004, doi: 10.1109/LSENS.2020.2996428.

[9] R. Pérez, F. Schubert, R. Rasshofer, and E. Biebl, "A machine learning joint lidar and radar classification system in urban automotive scenarios," *Advances in Radio Science: ARS*, vol. *17*, pp. 129-136, 2019

[10] *Mid-range radar sensor (MRR) for front and rear applications*, Robert Bosch GmbH.. Accessed on: Apr. 13, 2020. [Online]. Available: https://www.bosch-mobility-solutions.com/media/global/products-and-services/passenger-cars-and-light-commercial-vehicles/driver-assistance-systems/predictive-emergency-braking-system/mid-range-radar-sensor-(mrr)/product-data-sheet-mid-range-radar-sensor-(mrr)-2.pdf

[11] *ARS408-21 Premium Long Range Radar Sensor 77 GHz*, A.D.C. GmbH.. Accessed on: April 13, 2020. [Online]. Available: https://www.continental-automotive.com/getattachment/5430d956-1ed7-464b-afa3-cd9cdc98ad63/ARS408-21_datasheet_en_170707_V07.pdf.pdf

[12] A. Kamann, P. Held, F. Perras, P. Zaumseil, T. Brandmeier, and U. T. Schwarz, "Automotive radar multipath propagation in uncertain environments," in *2018 21st International Conference on Intelligent Transportation Systems (ITSC)*, pp. 859-864, Nov. 2018.

[13] Y. Cao, C. Xiao, B. Cyr, Y. Zhou, W. Park, S. Rampazzi, and Z. M. Mao, "Adversarial sensor attack on lidar-based perception in autonomous driving," in *2019 ACM SIGSAC Conference on Computer and Communications Security*, pp. 2267-2281, Nov. 2019.

[14] N. Kalra and S. M. Paddock, "Driving to safety: How many miles of driving would it take to demonstrate autonomous vehicle reliability?," *Transportation Research Part A: Policy and Practice*, vol. 94, pp. 182-193, 2016. Accessed on: April 13, 2020. [Online]. Available: doi: 10.1016/j.tra.2016.09.010

[15] P. Koopman and B. Osyk, "Safety argument considerations for public road testing of autonomous vehicles," *SAE Int. J. Adv. Curr. Pract. Mobil.*, vol. 1, no. 2, 2019.

[16] S. Heinrich, *Flash memory in the emerging age of autonomy*, Proceedings of the Flash Memory Summit, Santa Clara, CA, USA, pp. 7-10, 2017. Accessed on: Apr. 13, 2020. [Online]. Available: https://www.flashmemorysummit.com/English/Collaterals/Proceedings/2017/20170808_FT12_Heinrich.pdf

[17] S. Tuohy, M. Glavin, C. Hughes, E. Jones, M. Trivedi, and L. Kilmartin," Intra-Vehicle Networks: A Review," *IEEE Transactions on Intelligent Transportation Systems*, vol. 16, no. 2, pp. 534-545, Apr. 2015.

[18] L. van Dijk and G. Sporer, "Functional Safety for Automotive Ethernet Networks," *Journal of Traffic and Transportation Engineering*, vol. 6, no. 4, pp. 176-182. 2018. Accessed on: April 13, 2020. [Online]. Available: doi: 10.17265/2328-2142/2018.04.003

[19] H. Munenori, *An introduction to ultrasonic sensors for vehicle parking*, Murata Electronics (UK) Ltd., May 2010. Accessed on: April 13, 2020. Accessed on: April 13, 2020. [Online]. Available: https://www.newelectronics.co.uk/electronics-technology/an-introduction-to-ultrasonic-sensors-for-vehicle-parking/24966/

[20] H. Winner, S. Hakuli, F. Lotz and C. Singer, *Handbook of driver assistance systems: Basic Information, Components and Systems for Active Safety and Comfort*, Springer International Publishing, 2016.

[21] H. H. Meinel, "Evolving automotive radar — From the very beginnings into the future," in *The 8th European Conference on Antennas and Propagation (EuCAP 2014)*, The Hague, pp. 3107-3114, 2014.

[22] J. Wojtanowski, M. Zygmunt, M. Kaszczuk, Z. Mierczyk and M. Muzal, "Comparison of 905 nm and 1550 nm semiconductor laser rangefinders' performance deterioration due to adverse environmental conditions," *Opto-Electronics Review*, vol. 22, no. 3, pp. 183-190, 2014. Accessed on: April 13, 2020. [Online]. Available: doi: 10.2478/s11772-014-0190-2

[23] I. Veselovskii, D. N. Whiteman, M. Korenskiy, A. Suvorina, and D. Pérez-Ramírez, "Use of rotational Raman measurements in multiwavelength aerosol lidar for evaluation of particle backscattering and extinction," *Atmospheric Measurement Techniques*, vol. 8, no. 7, pp. 4111-4122, 2015. Accessed on: April 13, 2020. [Online]. Available: doi: 10.5194/amt-8-4111-2015

[24] K. Piniarski, P. Pawłowski, and A. Dąbrowski, "Pedestrian detection by video processing in automotive night vision system," *2014 Signal Processing: Algorithms, Architectures, Arrangements, and Applications (SPA)*, pp. 104-109, 2014.

[25] N. Pinchon, C. Olivier, N. Adrien, B. Frédéric, L. Patrick, T. Jean-Philippe, B. Roland, B. Emmanuel, and B. Johann, "All-weather vision for automotive safety: which spectral band?," *International Forum on Advanced Microsystems for Automotive Applications 2018*, pp. 3-15. 2018. Accessed on: April 13, 2020. [Online]. Available: doi: 10.1007/978-3-319-99762-9_1

[26] B. Pal and S. Khaiyum, "Recent advances in software, sensors and computation platforms used in Autonomous Vehicles, A Survey, " *Int.*

J. Res. Anal. Rev., vol. 6, no. 1, 2019, Accessed on: Nov. 22, 2018. [Online]. Available: doi: 10.1729/Journal.20181

[27] F. Hamrani and V. Le Troadec, *Bosch MPC2 - Forward Automotive Camera for Advanced Driver Assistance Systems: Bosch confirms its will to catch up on the forward camera market with a second issue of their multipurpose camera*, SystemPlus Consulting, 2017. Accessed on: Apr. 13, 2020. [Online]. Available: https://www.systemplus.fr/wp-content/uploads/2017/04/SP17324_Bosch_MPC2_Forward_Camera_Flyer_System_Plus_Consulting.pdf

[28] V. K. Kukkala, J. Tunnell, S. Pasricha, and T. Bradley, "Advanced Driver-Assistance Systems: A Path Toward Autonomous Vehicles," *IEEE Consum. Electron. Mag.*, vol. 7, no. 5, pp. 18–25, 2018, Accessed on: Apr. 13, 2020. [Online]. Available: doi: 10.1109/MCE.2018.2828440

[29] H. Huang, C. Lee, and H. Lin, "Nighttime vehicle detection and tracking base on spatiotemporal analysis using RCCC sensor," in *2017 IEEE 9th International Conference on Humanoid, Nanotechnology, Information Technology, Communication and Control, Environment and Management (HNICEM)*, pp. 1-5. IEEE, 2017.

[30] H. Phelippeau, M. Akil, B. Dias Rodrigues, H. Talbot, and S. Bara, "Bayer bilateral denoising on TriMedia3270", *Real-Time Image and Video Processing 2009*, 2009. Accessed on: Apr. 13, 2020. [Online]. Available: doi: 10.1117/12.812330

[31] L. Cruz, D. Lucio, and L. Velho, "Kinect and RGBD images: Challenges and applications," In *Proc. 25th SIBGRAPI - Conf. Graph. Patterns Images Tutorials SIBGRAPI-T 2012*, pp. 36–49, Jun. 2014. Accessed on: Apr. 13, 2020. [Online]. Available: doi: 10.1109/SIBGRAPI-T.2012.13

[32] A. Rogalski and K. Chrzanowski, "Infrared devices and techniques," *Handb. Optoelectron. Second Ed. Concepts, Devices, Tech.*, vol. 1, no. 2, pp. 111–136, 2002, Accessed on: Apr. 13, 2020. [Online]. Available: doi: 10.1201/9781315157009

[33] *ADASKY White paper: How Far Infrared (FIR) Technology Enables 24/7 Autonomous Driving in Any Condition*, AdaSky, 2018. Accessed on: Apr. 13, 2020. [Online]. Available: http://www.adasky.com/wp-content/uploads/2018/03/White_paper_designed.pdf

[34] P. Kamencay, M. Breznan, R. Jarina, P. Lukac, and M. Zachariasova, "Improved depth map estimation from stereo images based on hybrid method," *Radioengineering*, vol. 21, no. 1, pp. 79– 85, 2012.

[35] *Thermal Vision Automotive Development Kit (ADK) FLIR ADK™*, FLIR® Systems, Inc., Wilsonville, 2019. Accessed on: Apr. 13, 2020. [Online]. Available: https://www.flir.co.uk/products/adk/

[36] *Thermal Imaging and Car Night Vision*, SATIR, 2020. Accessed on: Apr. 13, 2020. [Online]. Available: https://satir.com/application/thermal-imaging-and-car-night-vision

[37] *Lanmodo Vast—1080P Automotive Night Vision System*, lanmodo.com, 2020. Accessed on: Apr. 13, 2020. [Online]. Available: https://www.lanmodo.com/lanmodo-1080p-automotive-night-vision-system.html

[38] P. Hosur, R. B. Shettar and M. Potdar, "Environmental awareness around vehicle using ultrasonic sensors," in *2016 International Conference on Advances in Computing, Communications and Informatics (ICACCI)*, Jaipur, pp. 1154-1159, 2016.

[39] *Ultrasonic Sensor*, Robert Bosch GmbH.. Accessed on: Apr. 13, 2020. [Online]. Available: https://www.bosch-mobility-solutions.com/en/products-and-services/passenger-cars-and-light-commercial-vehicles/driver-assistance-systems/construction-zone-assist/ultrasonic-sensor/

[40] V. Agarwal, N. Murali and C. Chandramouli, "A Cost-Effective Ultrasonic Sensor-Based Driver-Assistance System for Congested Traffic Conditions," *IEEE Transactions on Intelligent Transportation Systems*, vol. 10, no. 3, pp. 486-498, 2009. Accessed on: Apr. 13, 2020. [Online]. Available: 10.1109/tits.2009.2026671 [Accessed: Apr. 13, 2020].

[41] *Ultrasonic Sensor FAQs - Senix (Distance and Level Sensors)*, Senix Distance and Level Sensors, 2020. Accessed on: Apr. 13, 2020. [Online]. Available: https://senix.com/ultrasonic-sensor-faqs/

[42] *Why are automotive radar systems moving from 24GHz to 77GHz?*, Texas Instruments, 2020. Accessed on: Apr. 13, 2020. [Online]. Available: https://e2e.ti.com/blogs_/b/behind_the_wheel/archive/2017/10/25/why-are-automotive-radar-systems-moving-from-24ghz-to-77ghz

[43] V. Winkler. "Range Doppler detection for automotive FMCW radars." in *2007 European Radar Conference*, pp. 166-169. IEEE, 2007.

[44] H. Eugin and J. Lee. "A meothod for multi-target range and velocity detection in automotive FMCW radar." in *2009 12th International IEEE Conference on Intelligent Transportation Systems*, pp. 1-5. IEEE, 2009.

[45] M. Jokela, M. Kutila, and P. Pyykönen, "Testing and Validation of Automotive Point-Cloud Sensors in Adverse Weather Conditions," *Applied Sciences*, vol. 9, no. 11, p. 2341, 2019. Accessed on: Apr. 13, 2020. [Online]. Available: doi: 10.3390/app9112341

[46] *Metawave Successfully Demonstrates 300 Meter Radar on Infineon Platform*, Businesswire.com, 2020. Accessed on: Apr. 13, 2020. [Online]. Available: https://www.businesswire.com/news/home/20181009005331/en/Metawave-Successfully-Demonstrates-300-Meter-Radar-Infineon

[47] E. Hyun, Y. Jin, and J. Lee, "A Pedestrian Detection Scheme Using a Coherent Phase Difference Method Based on 2D Range-Doppler FMCW Radar," *Sensors*, vol. 16, no. 1, p. 124, 2016. Accessed on: Apr. 13, 2020. [Online]. Available: doi: 10.3390/s16010124

[48] B. Jonathan, T. Foote, J. Keller, A. Kushleyev, D. Lee, A. Stewart, P. Vernaza, J. Derenick, J. Spletzer, and B. Satterfield. "Little ben: The ben franklin racing team's entry in the 2007 DARPA urban challenge," *Journal of Field Robotics* 25, no. 9, pp. 598-614, 2008.

[49] C. Rablau, "LiDAR - A new (self-driving) vehicle for introducing optics to broader engineering and non-engineering audiences", *Optics InfoBase Conference Papers*, Part F130-ETOP 2019, pp. 1–14, 2019. Accessed on: Apr. 13, 2020. [Online]. Available: doi: 10.1117/12.2523863.

[50] A. Martin, D. Dodane, L. Leviandier, D. Dolfi, A. Naughton, P. O'Brien, T. Spuessens, R. Baets, G. Lepage, P. Verheyen, P. De Heyn, P. Absil, P. Feneyrou, and J. Bourderionnet, "Photonic integrated circuit-based FMCW coherent LiDAR," *Journal of Lightwave Technology* 36, no. 19, pp. 4640-4645, 2018.

[51] T.B. Lee, *How 10 leading companies are trying to make powerful, low-cost lidar*, Condé Nast, 2019. Accessed on: Apr. 13, 2020. [Online]. Available: https://arstechnica.com/cars/2019/02/the-ars-technica-guide-to-the-lidar-industry/

[52] J. Maria, M. Kutila, and P. Pyykönen, "Testing and Validation of Automotive Point-Cloud Sensors in Adverse Weather Conditions," *Applied Sciences*, vol. 9, no. 11, pp.2341, 2019

[53] *The Automotive LiDAR Market*, Woodside Capital Partners, Yole Développement, Apr. 2018. Accessed on: Apr. 13, 2020. [Online]. Available: http://www.woodsidecap.com/wp-content/uploads/2018/04/Yole_WCP-LiDAR-Report_April-2018-FINAL.pdf

[54] *XenoLidar*, XenomatiX. Accessed on: Apr. 13, 2020. [Online]. Available: https://www.xenomatix.com/lidar/xenolidar/

[55] RS-LiDAR-32, Robosense. Accessed on: Apr. 13, 2020. [Online]. Available: https://www.robosense.ai/rslidar/rs-lidar-32

[56] *AE200*, AEye, Inc.. Accessed on: Apr. 13, 2020. [Online]. Available: https://www.aeye.ai/products/#ae200-product-description

[57] W. Nilushi and K. Ghaffarzadeh, "Lidar 2020-2030: Technologies, Players, Markets & Forecasts," *IDTechEx*. 2020

[58] C.V. Poulton, "Integrated LIDAR with optical phased arrays in silicon photonics," PhD diss., Massachusetts Institute of Technology, 2016.

[59] National Transportation Safety Board, "Rear-End Collision Between a Car Operating with Advanced Driver Assistance Systems and a Stationary Fire Truck, Culver City, California, January 22, 2018," *National Transportation Safety Board*, HAB1907, 2019. Accessed on: Apr. 7, 2020. [Online]. Available: https://www.ntsb.gov

[60] J. Hecht, "Lidar for Self-Driving Cars," *Optics & Photonics News*, pp. 26–33, Jan. 2018.

[61] M. Michaelis, P. Berthold, D. Meissner, and H. J. Wuensche, "Heterogeneous multi-sensor fusion for extended objects in automotive scenarios using Gaussian processes and a GMPHD-filter," in *2017 Sensor Data Fusion: Trends, Solutions, Applications (SDF)* IEEE. pp. 1-6, Oct. 2017.

[62] F. C. Delori, R. H. Webb, and D. H. Sliney, "Maximum permissible exposures for ocular safety (ANSI 2000), with emphasis on ophthalmic devices, " *J. Opt. Soc. Am. A*, vol. 24, no. 5, pp. 1250–1265, 2007.

[63] S. Randall, *Working with lasers: Updated to include IEC:2014*, Laser Safety O.S., 2016. Accessed on: Apr. 13, 2020. [Online]. Available:https://slideplayer.com/slide/12202834/

[64] M. Kutila, P. Pyykönen, H. Holzhüter, M. Colomb and P. Duthon, "Automotive LiDAR performance verification in fog and rain," *2018* in *21st International Conference on Intelligent Transportation Systems (ITSC)*, Maui, HI, USA, pp. 1695-1701, 2018. Accessed on: Apr. 13, 2020. [Online]. Available: doi: 10.1109/ITSC.2018.8569624.

[65] R. Günther, L. Liu, D. Liang, R. Jones, A. Fang, B. Koch, and J.

Bowers, "III-V/silicon photonics for on-chip and intra-chip optical interconnects," *Laser & Photonics Reviews*, vol 4, no. 6, pp. 751-779, 2010.

[66] A.E. Lim, J. Song, Q. Fang, C. Li, X. Tu, N. Duan, K.Chen, R. P. Tern, and T. Liow, "Review of silicon photonics foundry efforts," *IEEE Journal of Selected Topics in Quantum Electronics*, vol. 20, no. 4, pp. 405-416, 2013.

[67] S.T. Fard, K. Murray, M. Caverley, V. Donzella, J. Flueckiger, S.M. Grist, E. Huante-Ceron, S.A. Schmidt, E. Kwok, N.A. Jaeger, A. P. Knights, and L. Chrostowski, "Silicon-on-insulator sensors using integrated resonance-enhanced defect-mediated photodetectors," *Optics express*, vol. 22, no. 23, pp. 28517-28529, 2014.

[68] R. Soref, "Mid-infrared photonics in silicon and germanium," *Nature photonics*, vol 4, no. 8, pp. 495, 2010

[69] M. Bijelic, T. Gruber, and W. Ritter, "A Benchmark for Lidar Sensors in Fog: Is Detection Breaking Down?, " *IEEE Intelligent Vehicles Symposium, Proceedings*, vol 4, pp. 760–767, IEEE, Jun. 2018. Accessed on: Apr. 13, 2020. [Online]. Available: doi: 10.1109/IVS.2018.8500543

[70] J. Maria, M. Kutila, and P. Pyykönen, "Testing and Validation of Automotive Point-Cloud Sensors in Adverse Weather Conditions," *Applied Sciences*, vol. 9, no. 11, pp. 2341, 2019.

[71] P. Duthon, M. Colomb, and F. Bernardin, "Light Transmission in Fog: The Influence of Wavelength on the Extinction Coefficient," *Applied Sciences*, vol. 9, no.14, pp. 2843. 2019. Accessed on: Apr. 13, 2020. [Online]. Available: doi: 10.3390/app9142843

[72] J. Wojtanowski, M. Zygmunt, M. Kaszczuk, Z. Mierczyk, and M. Muzal, "Comparison of 905 nm and 1550 nm semiconductor laser rangefinders' performance deterioration due to adverse environmental conditions," *Opto-Electron.Rev.* vol. 22, no. 3, pp. 183–190, 2014. Accessed on: Apr. 13, 2020. [Online]. Available: doi: 10.2478/s11772-014-0190-2

[73] S. Royo and M. Ballesta-Garcia, "An Overview of Lidar Imaging Systems for Autonomous Vehicles," *Appl. Sci*., vol. 9, pp. 4093, 2019.

[74] *HDL64E User's Manual and Programming guide*, Velodyne Lidar, Inc.. Accessed on: Apr. 13, 2020. [Online]. Available: https://velodynelidar.com/downloads/

[75] G. J. Ayers, M. A. Ciampa, and N. A. Vranos, "Holographic Optical Beam Steering Demonstration, " in *Proceedings of the IEEE Photonic Society 24th Annual Meeting*, Arlington, VA, USA, vol. 9, no. 13, pp. 361–362, Oct. 2011.

[76] E. Ackerman, "Hail, robo-taxi!," *IEEE Spec.*, vol. 54, pp. 26–29, 2017.

[77] Ç. Ataman, S. Lani, W. Noell, and N. De Rooij, "A dual-axis pointing mirror with moving-magnet actuation," *J. Micromech. Microeng.*, vol. 23, 2012.

[78] L. Ye, G. Zhang, and Z. You, "5 V compatible two-axis PZT driven MEMS scanning mirror with mechanical leverage structure for miniature LiDAR application," *Sensors*, vol. 17, pp. 521, 2017.

[79] INNOVIZ ONE Automotive-Grade Solid-State LiDAR, Innoviz Technologies Ltd.. Accessed on: Apr. 13, 2020. [Online]. Available: https://innoviz.tech/innovizone/

[80] H. Schenk, P. Durr, T. Haase, D. Kunze, U. Sobe, H. Lakner, and H. Kuck, "Large deflection micromechanical scanning mirrors for linear scans and pattern generation," *IEEE J. Sel. Top. Quantum Electron.*, vol. 6, pp. 715–722, 2000.

[81] B. L. Stann, J. F. Dammann, and M. M. Giza, "Progress on MEMS-scanned ladar," *Proceedings of the Laser Radar Technology and Applications XXI*, SPIE: Bellingham, WA, USA, pp. 9832, 2016.

[82] H. W. Yoo, N. Druml, D. Brunner, C. Schwarzl, T. Thurner, M. Hennecke, and G. Schitter. "MEMS-based lidar for autonomous driving," *Elektrotech. Inftech.,* vol. 135, no. 6, pp. 408-415, 2018.

[83] G. Kim, J. Eom, and Y. Park, "Design and implementation of 3d lidar based on pixel-by-pixel scanning and ds-ocdma," *Smart Photonic and Optoelectronic Integrated Circuits XIX*, SPIE: Bellingham, WA, USA, pp. 10107, 2017.

[84] Lidar Sensor, Infineon Technologies AG., Accessed on: Apr. 13, 2020. [Online]. Available: https://www.infineon.com/cms/en/product/sensor/radar-image-sensors/lidar-sensors/

[85] M. E. Warren, "Automotive LIDAR Technology," *2019 Symposium on VLSI Circuits*, Kyoto, Japan, 2019, pp. C254-C255.

[86] J. D. Weinberg, R. Dissly, D. Nicks, and K. L. Miller, "Applications and field testing of a flash lidar system for future planetary missions," in *Lunar and Planetary Science Conference*, vol. 40, 2009.

[87] U. Yutaka, T. Horikawa, T. Nakamura, and Y. Arakawa, "Photonics-electronics convergence system for high density inter-chip interconnects by using silicon photonics," in *2012 IEEE Compound Semiconductor Integrated Circuit Symposium (CSICS)*, IEEE, pp. 1-4, 2012.

[88] M. Lipson, "Guiding, modulating, and emitting light on silicon-challenges and opportunities," *Journal of Lightwave Technology*, vol. 23, no. 12, pp. 4222, 2005.

[89] V. Donzella, A. Sherwali, J. Flueckiger, S. M. Grist, S. T. Fard, and L. Chrostowski, "Design and fabrication of SOI micro-ring resonators based on sub-wavelength grating waveguides," *Optics express*, vol. 23, no. 4, pp. 4791-4803, 2015.

[90] E. Luan, V. Donzella, K. Cheung, and L. Chrostowski, "Advances in Silicon Photonic Sensors Using Sub-Wavelength Gratings," in *2019 24th OptoElectronics and Communications Conference (OECC) and 2019 International Conference on Photonics in Switching and Computing (PSC)*, pp. 1-3. IEEE, 2019.

[91] M.R. Watt, *A review of Optical Phased Array LiDAR: Silicon Photonics Phased Array LiDAR*, AutoSens Brussels, 2018. Accessed on: Apr. 13, 2020. [Online]. Available: https://www.youtube.com/watch?v=H-ZYe2IONOs&feature=youtu.be

[92] R. Soref, "The past, present, and future of silicon photonics," *IEEE Journal of selected topics in quantum electronics*, vol. 12, no. 6, pp. 1678-1687, 2006.

[93] M. Hochberg and T. Baehr-Jones, "Towards fabless silicon photonics," *Nature Photonics*, vol. 4, no. 8, pp.492-494, 2010.

[94] W. Bogaerts, "Design challenges in large-scale silicon photonics," in *13th International Conference on Numerical Simulation of Optoelectronic devices (NUSOD 2013)*, 2013, p. 63-64.

[95] P. F. McManamon, T. A. Dorschner, D. L. Corkum, L. J. Friedman, D. S. Hobbs, M. Holz, S. Liberman, H.Q. Nguyen, D.P. Resler, R.C. Sharp, and E.A. Watson, "Optical phased array technology," *Proceedings of the IEEE*, vol. 84, no. 2, pp. 268-298, 1996.

[96] J. Riu and S. Royo, "A compact long-range lidar imager for high spatial operation in daytime," in *Proceedings of the 8th International Symposium on Optronics in Defence and Security*, 3AF—The French Aerospace Society: Paris, France, 2018, pp. 1–4.

[97] M. Heck, "Highly integrated optical phased arrays: photonic integrated circuits for optical beam shaping and beam steering," *Nanophotonics*, vol. 6, no. 1, pp. 93-107, 2016. Accessed on: Apr. 13, 2020. [Online]. Available: doi: 10.1515/nanoph-2015-0152.

[98] R. Hansen, *Phased array antennas*. Chichester, West Sussex: Wiley, 2009.

[99] D. N. Hutchison, J. Sun, J. K. Doylend, R. Kumar, J. Heck, W. Kim, C. T. Phare, A. Feshali, and H. Rong, "High-resolution aliasing-free optical beam steering," *Optica*, vol. 3, pp. 887–890, 2016.

[100] F. Vasey, F. Reinhart, R. Houdré and J. Stauffer, "Spatial optical beam steering with an AlGaAs integrated phased array", *Applied Optics*, vol. 32, no. 18, p. 3220, 1993.

[101] C. V. Poulton, M. Byrd, M. Raval, Z. Su, N. Li, E. Timurdogan, D. Coolbaugh, D. Vermeulen, and M. Watts, "Large-scale silicon nitride nanophotonic phased arrays at infrared and visible wavelengths", *Optics Letters*, vol. 42, no. 1, p. 21, 2016. Accessed on: Apr. 13, 2020. [Online]. Available: doi: 10.1364/ol.42.000021.

[102] Y. Zhang, Y. Ling, Y. Zhang, K. Shang, and S. J. Ben Yoo, "High-density wafer-scale 3-D silicon-photonic integrated circuits," *IEEE Journal of Selected Topics in Quantum Electronics*, vol. 24, no. 6, pp. 1-10, 2018.

[103] C. T. Phare, M. C. Shin, S. A. Miller, B. Stern, and M. Lipson. "Silicon optical phased array with high-efficiency beam formation over 180 degree field of view," *arXiv preprint*, 2018. Accessed on: Apr. 13, 2020. [Online]. Available: arXiv:1802.04624

[104] C. V. Poulton, M. J. Byrd, P. Russo, E. Timurdogan, M. Khandaker, D. Vermeulen, and M. R. Watts, "Long-range LiDAR and free-space data communication with high-performance optical phased arrays," *IEEE Journal of Selected Topics in Quantum Electronics*, vol. 25, no. 5, pp. 1-8, 2019.

[105] B. J. Frey, D. B. Leviton, and T. J. Madison, "Temperature-dependent refractive index of silicon and germanium," *Optomechanical technologies for Astronomy*, vol. 6273, International Society for Optics and Photonics, 2006.

[106] C. V. Poulton, P. Russo, E. Timurdogan, M. Whitson, M. J. Byrd, E. Hosseini, B. Moss, Z. Su, D. Vermeulen, and M. R. Watts, "High-performance integrated optical phased arrays for chip-scale beam steering and lidar," *CLEO: Applications and Technology*, Optical Society of America, 2018.

[107] L. Chrostowski and M. Hochberg, *Silicon photonics design: from devices to systems*. Cambridge University Press, 2015.
[108] J. Witzens, "High-speed silicon photonics modulators," *Proceedings of the IEEE*, vol 106, no. 12, pp. 2158-2182, 2018.
[109] L. Qiao, W. Tang, and T. Chu, "32× 32 silicon electro-optic switch with built-in monitors and balanced-status units," *Scientific Reports*, vol. 7, no. 1, pp. 1-7, 2017.
[110] K. Van Acoleyen, W. Bogaerts, J. Jágerská, N. Le Thomas, R. Houdré, and R. Baets, "Off-chip beam steering with a one-dimensional optical phased array on silicon-on-insulator," *Optics Letters*, vol. 34, no. 9, pp. 1477, 2009. Accessed on: Apr. 13, 2020. [Online]. Available: doi: 10.1364/ol.34.001477
[111] D. Kwong, A. Hosseini, Y. Zhang, and R. Chen, "1 × 12 Unequally spaced waveguide array for actively tuned optical phased array on a silicon nanomembrane", *Applied Physics Letters*, vol. 99, no. 5, 2011. Accessed on: Apr. 13, 2020. [Online]. Available: doi: 10.1063/1.3619847.
[112] K. Van Acoleyen, K. Komorowska, W. Bogaerts, and R. Baets, "One-Dimensional Off-Chip Beam Steering and Shaping Using Optical Phased Arrays on Silicon-on-Insulator," *Journal of Lightwave Technology*, vol. 29, no. 23, pp. 3500-3505, 2011. Accessed on: Apr. 13, 2020. [Online]. Available: doi:10.1109/jlt.2011.2171477
[113] J. Doylend, M. Heck, J. Bovington, J. Peters, L. Coldren, and J. Bowers, "Two-dimensional free-space beam steering with an optical phased array on silicon-on-insulator", *Optics Express*, vol. 19, no. 22, pp. 21595, 2011. Accessed on: Apr. 13, 2020. [Online]. Available: doi: 10.1364/oe.19.021595.
[114] K. Van Acoleyen, W. Bogaerts, and R. Baets, "Two-Dimensional Dispersive Off-Chip Beam Scanner Fabricated on Silicon-On-Insulator", *IEEE Photonics Technology Letters*, vol. 23, no. 17, pp. 1270-1272, 2011. Accessed on: Apr. 13, 2020. [Online]. Available: doi: 10.1109/lpt.2011.2159785
[115] J. K. Doylend, M. J. R. Heck, J. T. Bovington, J. D. Peters, M. L. Davenport, L. A. Coldren, and J. E. Bowers, "Hybrid III/V silicon photonic source with integrated 1D free-space beam steering", *Optics Letters*, vol. 37, no. 20, pp. 4257, 2012. Accessed on: Apr. 13, 2020. [Online]. Available: doi: 10.1364/ol.37.004257
[116] J. Sun, E. Timurdogan, A. Yaacobi, E. Hosseini, and M. Watts, "Large-scale nanophotonic phased array," *Nature*, vol. 493, no. 7431, pp. 195-199, 2013. Accessed on: Apr. 13, 2020. [Online]. Available: doi: 10.1038/nature11727
[117] J. Sun, E. Hosseini, A. Yaacobi, D. B. Cole, G. Leake, D. Coolbaugh, and M. R. Watts, "Two-dimensional apodized silicon photonic phased arrays," *Optics Letters*, vol. 39, no. 2, pp. 367, 2014. Accessed on: Apr. 13, 2020. [Online]. Available: doi: 10.1364/ol.39.000367
[118] D. Kwong, A. Hosseini, J. Covey, Y. Zhang, X. Xu, H. Subbaraman, R. T. Chen, "On-chip silicon optical phased array for two-dimensional beam steering," *Optics Letters*, vol. 39, no. 4, pp. 941, 2014. Accessed on: Apr. 13, 2020. [Online]. Available: doi: 10.1364/ol.39.000941
[119] A. Yaacobi, J. Sun, M. Moresco, G. Leake, D. Coolbaugh, and M. Watts, "Integrated phased array for wide-angle beam steering," *Optics Letters*, vol. 39, no. 15, pp. 4575, 2014. Accessed on: Apr. 13, 2020. [Online]. Available: doi: 10.1364/ol.39.004575.
[120] K. Wang, Y. Wang, S. Gao, A. Nirmalathas, C. Lim, K. Alameh, and E. Skafidas, "2×2 Silicon Integrated Optical Phased Array for Beam Steering Applications," in *Proc. of MWP*, 2015, pp. 1-4.
[121] J. C. Hulme, J. K. Doylend, M. J. R. Heck, J. D. Peters, M. L. Davenport, J. T. Bovington, L. A. Coldren, and J. E. Bowers, "Fully integrated hybrid silicon two dimensional beam scanner," *Optics Express*, vol. 23, no. 5, pp. 5861, 2015. Accessed on: Apr. 13, 2020. [Online]. Available: doi: 10.1364/oe.23.005861
[122] B. Guan, C. Qin, R. P. Scott, B. Ercan, N. K. Fontaine, T. Su, and S. J. B. Yoo, "Hybrid 3D photonic integrated circuit for optical phased array beam steering, " *CLEO: Science and Innovations*, pp. 10–15, May 2015.
[123] H. Abediasl and H. Hashemi, "Monolithic optical phased-array transceiver in a standard SOI CMOS process", *Optics Express*, vol. 23, no. 5, p. 6509, 2015. Accessed on: Apr. 13, 2020. [Online]. Available: doi: 10.1364/oe.23.006509
[124] F. Aflatouni, B. Abiri, A. Rekhi, and A. Hajimiri, "Nanophotonic projection system", *Optics Express*, vol. 23, no. 16, pp. 21012, 2015. Accessed on: Apr. 13, 2020. [Online]. Available: 10.1364/oe.23.021012.
[125] C. V. Poulton, A.Yaacobi, D. B. Cole, M. J. Byrd, M. Raval, D. Vermeulen, and M. R. Watts, "Coherent solid-state LIDAR with silicon photonic optical phased arrays," *Optics Letters*, vol. 42, no. 20, pp. 4091, 2017. Accessed on: Apr. 13, 2020. [Online]. Available: doi: 10.1364/ol.42.004091.
[126] S. Chung, H. Abediasl, and H. Hashemi, "A Monolithically Integrated Large-Scale Optical Phased Array in Silicon-on-Insulator CMOS," *IEEE Journal of Solid-State Circuits*, vol. 53, no. 1, pp. 275-296, 2018. Accessed on: Apr. 13, 2020. [Online]. Available: 10.1109/jssc.2017.2757009
[127], C. T. Phare, Y. Chang, X. Ji, O.A. Jimenez Gordillo, A. Mohanty, S. P. Roberts, M. C. Shin, B. Stern, M. Zadka, and M. Lipson, "512-element actively steered silicon phased array for low-power LIDAR," in *Conf. Lasers Electro-Opt.*, 2018, Paper JTh5C.2.
[128] Y. Zhang, Y. C. Ling, K. Zhang, C. Gentry, D. Sadighi, G. Whaley, J. Colosimo, P. Suni, and S. B. Yoo., "Sub-wavelength-pitch silicon-photonic optical phased array for large field-of-regard coherent optical beam steering," *Optics Express*, vol. 27, no. 3, pp. 1929-1940, 2019. Accessed on: Jul. 21, 2020. [Online]. Available: doi: 10.1364/oe.27.001929
[129] N. A. Tyler, D. Fowler, S. Malhouitre, S. Garcia, P. Grosse, W. Rabaud, and B. Szelag, "SiN integrated optical phased arrays for two-dimensional beam steering at a single near-infrared wavelength," *Optics Express*, vol. 27, no. 4, pp. 5851, 2019. Accessed on: Apr. 13, 2020. [Online]. Available: doi: 10.1364/oe.27.005851
[130] W. Xu, L. Zhou, L. Lu, and J. Chen, "Aliasing-free optical phased array beam-steering with a plateau envelope," *Optics Express*, vol. 27, no. 3, pp. 3354, 2019. Accessed on: Apr. 13, 2020. [Online]. Available: doi: 10.1364/oe.27.003354
[131] R. Fatemi, A. Khachaturian, and A. Hajimiri, "A Nonuniform Sparse 2-D Large-FOV Optical Phased Array With a Low-Power PWM Drive", *IEEE Journal of Solid-State Circuits*, vol. 54, no. 5, pp. 1200-1215, 2019. Accessed on: Apr. 13, 2020. [Online]. Available: doi: 10.1109/jssc.2019.2896767
[132] M. I. Skolnik, "Introduction to Radar Systems McGraw-Hill," *New York*, vol:19622, pp.38, 1962.
[133] T. Komljenovic, R. Helkey, L. Coldren, and J. E. Bowers, "Sparse aperiodic arrays for optical beam forming and LIDAR," *Optics Express*, vol. 25, no. 3, pp. 2511-2528, 2017. Accessed on: Jul. 21, 2020. [Online]. Available: doi: 10.1364/oe.25.002511
[134] F. Zhao, H. Jiang, and Z. Liu, "Recent development of automotive LiDAR technology, industry and trends," *Eleventh International Conference on Digital Image Processing (ICDIP 2019)*, International Society for Optics and Photonics., vol. 11179, pp. 4A, 2019. Accessed on: Jul. 21, 2020. [Online]. Available: doi: 10.1117/12.2540277
[135] M. Watts, *Optical Phased Array Technology*, Analog Photonics LLC., 2020. Accessed on: Apr. 13, 2020. [Online]. Available: http://www.analogphotonics.com/
[136] *Quanergy Solid State LiDAR Introduction*, Quanergy Systems, Jul. 2019. Accessed on: Apr. 13, 2020. [Online]. Available: https://youtu.be/n3S8Io0kZZs
[137] X. Sun, L. Zhang, Q. Zhang, and W. Zhang, "Si Photonics for Practical LiDAR Solutions," *Applied Sciences*, vol. 9, no. 20, pp. 4225, 2019. Accessed on: Apr. 13, 2020. [Online]. Available: doi: 10.3390/app9204225
[138] P. Muñoz, G. Micó, L.A. Bru, D. Pastor, D. Pérez, J.D. Doménech, J. Fernández, R. Baños, B. Gargallo, R. Alemany, and A.M. Sánchez, "Silicon nitride photonic integration platforms for visible, near-infrared and mid-infrared applications." *Sensors*, vol. 17, n. 9, pp. 2088, 2017.
[139] T. Kim, P. Bhargava, C. V. Poulton, J. Notaros, A. Yaacobi, and E. Timurdogan, C. Baiocco, N. Fahrenkopf, S. Kruger, T. Ngai, Y. Timalsina, "A Single-Chip Optical Phased Array in a Wafer-Scale Silicon Photonics/CMOS 3D-Integration Platform," *IEEE Journal of Solid-State Circuits*, vol. 54, no. 11, pp. 3061-3074, 2019. Accessed on: Jul. 21, 2020. [Online]. Available: doi: 10.1109/jssc.2019.2934601
[140] M. Raval, C.V. Poulton, M.R. Watts, "Unidirectional waveguide grating antennas with uniform emission for optical phased arrays", *Optics letters*, vol. 42, no. 13, pp. 2563-6, 2017.
[141] S. Kaushal, R. Cheng, M. Ma, A. Mistry, M. Burla, L. Chrostowski, J. Azaña, "Optical signal processing based on silicon photonics waveguide Bragg gratings.", *Frontiers of Optoelectronics*, vol. 11, no. 2, pp. 163-88, 2018.
[142] K. Shang, C. Qin, Y. Zhang, G. Liu, X. Xiao, S. Feng, and S. J. Yoo., "Uniform emission, constant wavevector silicon grating surface emitter for beam steering with ultra-sharp instantaneous field-of-view," *Optics Express*, vol. 25, no. 17, pp. 19655-19661, 2017. Accessed on: Jul. 21, 2020. [Online]. Available: doi: 10.1364/oe.25.019655
[143] H. Zhang, C. Li, X. Tu, H. Zhou, X. Luo, M. Yu, and G. Q. Lo., "High

Efficiency Silicon Nitride Grating Coupler with DBR," in *Optical Fiber Communication Conference 2014*, pp. 1-3, 2014. Accessed on: Jul. 21, 2020. [Online]. Available: doi: 10.1364/ofc.2014.th1a.4

[144] V. Donzella, S. Talebi Fard, and L. Chrostowski, "Study of waveguide crosstalk in silicon photonics integrated circuits," in *Photonics North 2013*, vol. 8915, pp.89150Z, 2013. Accessed on: Jul. 21, 2020. [Online]. Available: doi: 10.1117/12.2042366

[145] Y. Jin, A. Yan, Z. Hu, Z. Zhao, and W. Shi, "High speed and low side lobe optical phased array steering by phase correction technique," *Photonic Fiber and Crystal Devices: Advances in Materials and Innovations in Device Applications VII*, International Society for Optics and Photonics., vol. 8847, pp. 16 2013. Accessed on: Jul. 21, 2020. [Online]. Available: doi: 10.1117/12.2022611

[146] Z. Wang, A. Abbasi, U. Dave, A. De Groote, S. Kumari, B. Kunert, C. Merckling, M. Pantouvaki, Y Shi, B. Tian, and K. Van Gasse, "Novel light source integration approaches for silicon photonics.", *Laser & Photonics Reviews*, vol. 11, no.4, pp. 1700063, 2017.

[147] W. Guo, P. R. Binetti, C. Althouse, M. L. Masanovic, H. P. Ambrosius, L. A. Johansson, and L. A. Coldren, "Two-Dimensional Optical Beam Steering With InP-Based Photonic Integrated Circuits," *IEEE Journal of Selected Topics in Quantum Electronics*, vol. 19, no. 4, pp. 6100212-6100212, 2013. Accessed on: Jul. 21, 2020. [Online]. Available: doi: 10.1109/jstqe.2013.2238218

[148] J. Notaros, N. Li, C. V. Poulton, Z. Su, M. J. Byrd, E. S. Magden, E. Timurdogan, C. Baiocco, N. M. Fahrenkopf, and M. R. Watts, "CMOS-Compatible Optical Phased Array Powered by a Monolithically-Integrated Erbium Laser," *Journal of Lightwave Technology*, vol. 37, no. 24, pp. 5982-5987, 2019. Accessed on: Jul. 21, 2020. [Online]. Available: doi: 10.1109/jlt.2019.2944607

[149] N. Li, D. Vermeurlen, Z. Su, E. S. Magden, M. Xin, N. Singh, A. Ruocco, J. Nataros, C. V. Poulton, E. Timurdogan, C. Baiocco, and M. R. Watts, "Monolithically integrated erbium-doped tunable laser on a CMOS-compatible silicon photonics platform," *Optics Express*, vol. 26, no. 13, pp. 16200, 2018. Accessed on: Jul. 21, 2020. [Online]. Available: doi: 10.1364/oe.26.016200

[150] M. Tran, T. Komljenovic, D. Huang, L. Liang, M. Kennedy, and J. Bowers, "A Widely-Tunable High-SMSR Narrow-Linewidth Laser Heterogeneously Integrated on Silicon," in *Conference on Lasers and Electro-Optics*, 2018. Accessed on: Jul. 21, 2020. [Online]. Available: doi: 10.1364/cleo_at.2018.af1q.2

[151] R. Jones, P. Doussiere, J. B. Driscoll, W. Lin, H. Yu, Y. Akulova, T. Komljenovic, and J. E. Bowers, "Heterogeneously Integrated InP/Silicon Photonics: Fabricating Fully Functional Transceivers," *IEEE Nanotechnology Magazine*, vol. 13, no. 2, pp. 17-26, 2019. Accessed on: Jul. 21, 2020. [Online]. Available: doi: 10.1109/mnano.2019.2891369

[152] P. Bhargava, T. Kim, C. V. Poulton, J. Notaros, A. Yaacobi, E. Timurdogan, C. Baiocco, N. Fahrenkopf, S. Kruger, T. Ngai, and Y. Timalsina. "Fully integrated coherent LiDAR in 3D-integrated silicon photonics/65nm CMOS.," in *2019 Symposium on VLSI Circuits*, pp. C262-C263, 2019. Accessed on: Jul. 21, 2020. [Online]. Available: doi: 10.23919/VLSIC.2019.8778154

[153] P. Krochin-Yepez, U. Scholz, and A. Zimmermann, "CMOS-Compatible Measures for Thermal Management of Phase-Sensitive Silicon Photonic Systems," *Photonics*, vol. 7, no. 1, pp. 6, 2020. Accessed on: Jul. 21, 2020. [Online]. Available: doi: 10.3390/photonics7010006

[154] A. Rahim, J. Goyvaerts, B. Szelag, J. M. Fedeli, P. Absil, T. Aalto, M. Harjanne, C. Littlejohns, G. Reed, G. Winzer, and S. Lischke. "Open-Access Silicon Photonics Platforms in Europe", *IEEE Journal of Selected Topics in Quantum Electronics*, vol. 25, no. 5, pp. 1-8, 2019. Accessed on: Jul. 21, 2020. [Online]. Available: doi: 10.1109/jstqe.2019.2915949

[155] *LIGENTEC Foundry*, LIGENTEC SA, 2019. Accessed on: Jul. 21, 2020. [Online]. Available: https://www.ligentec.com/ligentec-foundry/

Ching-Pai Hsu received the M.S. degree (2012) in Engineering science and ocean engineering from National Taiwan University, Taipei, Taiwan,.

He is currently enrolled in the Smart, Connected and Autonomous Vehicle MSc at WMG, University of Warwick, UK. His research interests include design, fabrication, and characterization of photonic integrated circuits for optical phased array LiDAR application.

Boda Li received the BSc in Vehicle Engineering (2018) from Hunan University; the MSc degree (2019) from WMG, the University of Warwick.

He was a member of the China Society of Automotive Engineering from 2015. He is currently a Smart Connected and Autonomous Vehicle MSc student at WMG working on a project on RADAR interference.

Braulio Solano Rivas received his B.Eng. degree in Mechatronics from the Tecnologico de Costa Rica, Costa Rica, in 2018. During his BEng dissertation he developed an ADAS project at the Karlsruher Institut für Technologie (KIT), Germany.

He is currently an MSc student on Smart, Connected and Autonomous Vehicles at WMG, University of Warwick, and he has been awarded a WMG Excellence Scholarships. His M.Sc. dissertation is oriented on Visual Simultaneous Localization and Mapping (VSLAM).

Amar R. Gohil was born in UK, 1997. First-class Honours Bachelors in Mechanical Engineering, from Coventry University 2019.

He works at WMG, the University of Warwick, and he is currently an Associate Member of the Institute of Mechanical Engineering (AMIMechE).

Pak Hung Chan completed an integrated master's degree in mechanical engineering at the University of Warwick, UK, in 2018.

He is currently working as a Graduate Engineer at WMG, The University of Warwick, focusing on research around autonomous vehicles and perception sensors. He is also currently an Associate Member of IMechE.

Andrew D. Moore works as Principal Engineer in the Intelligent Vehicles group at WMG, University of Warwick, UK. His research interests are: RADAR, motor characterization, rail powertrains, power electronics and battery technology, wireless communications.

He previously worked as an electronics design engineer on robotics, LASERs, aviation test systems, particle size analyzers, ground RADAR, digital and analogue systems, wired communications and electro-optics and automation systems.

Valentina Donzella received her BSc (2003) and MSc (2005) in Electronics Engineering from University of Pisa and Sant'Anna School of Advanced Studies (Pisa, Italy), and her PhD (2010) in Innovative Technologies for Information, Communication and Perception Engineering from Sant'Anna School of Advanced Studies. In 2009, she was a visiting graduate student at McMaster University (Hamilton, ON, Canada) in the Engineering Physics department.

She is currently Associated Professor, in the Intelligent Vehicles group at WMG, University of Warwick, UK; before this position, she was a MITACS and SiEPIC postdoctoral fellow at the University of British Columbia (Vancouver, BC, Canada), in the Silicon Photonics group. She is first author and co-author of several journal papers on top tier optics journals. Her research interests are: LiDAR, Intelligent Vehicles, integrated optical sensors, sensor fusion, and silicon photonics.

Dr Donzella is Full College member of EPSRC and Senior Fellow of Higher Education Academy.